The Roles of Climate Variability on Runoff at Daily, Monthly, Annual, and Long-term Scales

Lili Yao[1], Dominic Libera[1], Marwan Mustafa A. Kheimi[1], Sankarasubramanian Arumugam[2], and Dingbao Wang[1]

[1]University of Central Florida
[2]North Carolina State University

November 26, 2022

Abstract

Climate variability, in terms of the climatic fluctuations in precipitation and potential evapotranspiration, impacts the variability of runoff at different timescales. This paper developed a new daily water balance model which unifies the probability distributed model and the SCS curve number method, and provides a unified framework for water balances across different timescales. The model uses a daily step but can be forced with climate inputs varying at different timescales. The model is applied to 82 MOPEX catchments, and the runoff at a coarser timescale is aggregated from the daily runoff. For runoff at each timescale, the relative role of each climate variability (daily, monthly, or inter-annual variability) is evaluated by comparing the modeled runoff forced with the climate variability at two consecutive timescales. It is found that the runoff variability at the daily, monthly, and annual scale is primarily controlled by the climate variability at the same timescale. The monthly climate variability significantly contributes to both the daily and inter-annual runoff variability. However, both daily and inter-annual climate variability play much smaller roles in monthly runoff variability. Besides monthly climate variability, mean annual runoff receives considerable contribution from the inter-annual climatic variability, which is often disregarded in previous studies. The quantitative evaluation of the roles of climate variability reveals how climate controls runoff across different timescales.

The Roles of Climate Variability on Runoff at Daily, Monthly, Annual, and Long-term Scales

Lili Yao[1], Dominic A. Libera[1], Marwan Kheimi[1], A. Sankarasubramanian[2], Dingbao Wang[1*]

[1]Department of Civil, Environmental, and Construction Engineering, University of Central Florida, Orlando, Florida, USA

[2]Department of Civil, Construction, and Environmental Engineering, North Carolina State University, Raleigh, NC, USA

[*]Correspondence to: dingbao.wang@ucf.edu

Abstract

Climate variability, in terms of the climatic fluctuations in precipitation and potential evapotranspiration, impacts the variability of runoff at different timescales. This paper developed a new daily water balance model which unifies the probability distributed model and the SCS curve number method, and provides a unified framework for water balances across different timescales. The model uses a daily step but can be forced with climate inputs varying at different timescales. The model is applied to 82 MOPEX catchments, and the runoff at a coarser timescale is aggregated from the daily runoff. For runoff at each timescale, the relative role of each climate variability (daily, monthly, or inter-annual variability) is evaluated by comparing the modeled runoff forced with the climate variability at two consecutive timescales. It is found that the runoff variability at the daily, monthly, and annual scale is primarily controlled by the climate variability at the same timescale. The monthly climate variability significantly contributes to both the daily and inter-annual runoff variability. However, both daily and inter-annual climate variability play much smaller roles in monthly runoff variability.

Besides monthly climate variability, mean annual runoff receives considerable contribution from the inter-annual climatic variability, which is often disregarded in previous studies. The quantitative evaluation of the roles of climate variability reveals how climate controls runoff across different timescales.

Keywords: Runoff, Climate variability, Inter-annual, Seasonality, Storminess, Budyko

Key points:

1. Runoff variations at the daily, monthly, and annual timescales are primarily affected by climate variability at the same timescale.
2. Monthly climate variability is the most important climatic fluctuation, followed by inter-annual variability, affecting mean annual runoff.
3. Monthly climate variability has significant effects on runoff at all the timescales.

1. Introduction

Understanding the climate's controls on catchment runoff at various timescales is of interest to hydrologists, earth system modelers, and water resources managers. Climate, soil, vegetation and topography all affect hydrological processes [*Eagleson*, 1978; *Farmer et al.*, 2003; *Troch et al.*, 2013]. The long-term mean and short-term fluctuations of climate exert a fundamental control on the water balance directly and indirectly. Climate variability can control the water balance differently at the daily, monthly and inter-annual timescales [*Jothityangkoon et al.*, 2001; *Atkinson et al.*, 2002, *Zhang et al.*, 2008]. As the two main variables of climate, precipitation serves as the water supply to the catchments from atmosphere, and potential evapotranspiration determines the water demand to the catchments. The effect of individual variability and co-variability of precipitation and potential evapotranspiration on runoff are dependent on the timescale at which the runoff is quantified.

Daily runoff variation is closely associated with daily climate fluctuations which are observed in the hydrographs for rainfall events. The variability of precipitation is much larger than that of potential evapotranspiration, and runoff dynamics at the daily scale are strongly controlled by the daily precipitation interacting with catchments characteristics, such as antecedent soil moisture [*Rodriguez-Iturbe et al.*, 1999; *Aubert et al.*, 2003; *Porporato et al.*, 2004; *Botter et al.*, 2007]. Antecedent soil moisture determines both the soil storage potential and infiltration capacity in catchments. Higher intensities of daily precipitation at lower frequencies create favorable conditions for runoff generation because of the limited soil retention and/or infiltration capacity [*Brutsaert*, 2005]. Monthly and inter-annual climatic fluctuations have impacts on daily runoff through direct changes in daily precipitation characteristics and through changes in antecedent soil moisture conditions [*Sivapalan, et al.*, 2005; *Berghuijs et al.*, 2014, 2016; *Perdigão and Blöschl*, 2014; *Rossi et al.*, 2015]. For example, on the first day of each month (or year), the runoff generation can be different for a given daily precipitation due to the different legacy soil moisture from the previous month (or year). Soil water storage capacity provides catchments resilience to climate perturbations [*McNamara et al.*, 2011]. The variation in groundwater storage regulates the storm water storage space and the antecedent soil wetness condition [*Troch et al.*, 1993; *Soylu et al.*, 2011; *Appels et al.*, 2017], and it has exhibited both significant seasonal and inter-annual variations because of the temporal fluctuations of recharge from precipitation [*Fan et al.*, 2007; *Jasechko et al.*, 2014; *McMillan and Srinivasan*, 2015]. Therefore, in order to fully capture the variation of daily runoff, it is required to identify the impacts of climate variabilities at different timescales.

Monthly variations in precipitation and potential evapotranspiration are crucial characteristics of climate and are largely responsible for the runoff variability at the monthly scale [*Dettinger and Diaz*, 2000; *Yokoo et al.*, 2008; *Yaeger et al.*, 2012; *Berghuijs et al.*, 2014]. Monthly variations in precipitation and potential evapotranspiration are usually described as sinusoidal functions with certain phase shifts [*Milly*, 1994; *Woods*, 2009]. The correlation between precipitation and potential evapotranspiration has significant impacts on the monthly runoff. Runoff seasonality can be weak when precipitation and potential evapotranspiration are in phase because the peak of water supply and water demand occur in the same month(s) even though both of them have a strong seasonality. On the other hand, if precipitation and potential evapotranspiration are out of phase, the peak of runoff can be largely determined by the seasonality of precipitation because the peak of water supply coincides with the lowest water demand [*Petersen et al.*, 2012; *Berghuijs et al.*, 2014]. Inter-annual climate variability also has an impact on the monthly water balance by controlling the antecedent soil moisture through storage carryover in catchments [*Chen et al.*, 2013]. Additionally, the number of rainfall events and the time intervals between rainfall events at the daily scale influence the cumulative runoff at the monthly scale as well [*Appels et al.*, 2017].

Inter-annual variation in the water balance has been investigated in many studies [*Koster and Suarez*, 1999; *Arora*, 2002; *Yang et al.*, 2007; *Istanbulluoglu et al.*, 2012; *Han et al.*, 2018]. It has been found that the inter-annual variability in runoff is mainly controlled by the inter-annual variability of climate, especially in humid regions [*Milly and Dunne*, 2002; *Yang et al.*, 2006; *Xu et al.*, 2012]. Monthly climate variability is also an important determinant of the inter-annual variations in runoff [*Milly and Dunne*, 2002; *Potter and Zhang*, 2009; *Jothityangkoon et al.*, 2009]. For example, the same annual precipitation depth could produce different amounts of runoff if precipitation is concentrated on just several months compared to if precipitation is evenly distributed across all the months. The impacts of daily storminess could also propagate to the annual runoff, especially in dry catchments [*Zanardo et al.*, 2012].

Mean annual water balances are mainly determined by the long-term mean climate condition in terms of climate aridity index, defined as the ratio between mean annual potential evapotranspiration and precipitation. The first-order control of the mean climate on the mean annual runoff has been widely demonstrated in the Budyko framework [*Budyko*, 1958, 1974; *Milly*, 1994; *Zhang et al.*, 2001; *Yang et al.*, 2008; Gentine *et al.*, 2012]. The scatter of catchments around the original Budyko curve has been interpreted as the result of short-term climate variability and varying catchment characteristics such as vegetation, soil and topography [*Fu*, 1981; *Porporato et al.*, 2004; *Donohue et al.*, 2007; *Li et al.*, 2013]. Daily precipitation with a larger variance tends to increase mean annual runoff [*Shao et al.*, 2012], though it has been found the effects of daily storminess are almost negligible when the infiltration excess runoff is not prevalent [*Reggiani et al.*, 2000]. Several studies have shown that runoff tends to be smaller for a given mean annual precipitation when the precipitation and potential evapotranspiration are in phase, and larger when they are out of phase [*Milly*, 1994; *Hickel and Zhang*, 2006; *Feng et al.*, 2012; *Petersen et al.*, 2012]. However, the opposite could be observed because infiltration excess runoff can contribute significant volumes of runoff in catchments when the precipitation and potential evapotranspiration are in phase [*Potter et al.*, 2005]. The influence of inter-annual climate variability on mean annual runoff is often disregarded even though it has been justified that the inter-annual variability of precipitation and potential evapotranspiration reduces the mean annual evaporation and increases the mean annual runoff [*Li*, 2014].

Existing studies have recognized that runoff, at each timescale, receives direct and indirect influences from climate variability at various timescales. However, these studies have focused on runoff at one or two timescales, the mean climate and/or individual climate variability (e.g., monthly variability), or a few catchments with similar climate. Therefore, a fundamental research question still remains unresolved: What are the relative magnitudes of the impacts of different climate variabilities on each timescale runoff under different climatic regimes? For example, for the daily runoff, which timescale climate variability plays the most predominant role on the runoff variation?, and what are the relative magnitudes of the impacts exerted by daily, monthly, and inter-annual climate variability on the daily runoff?

The major purpose of this paper is to systematically quantify the relative roles of daily, monthly, and inter-annual variability in precipitation (P) and potential evapotranspiration (E_p) on the runoff at four timescales, i.e., daily, monthly, annual and long-term. Additionally, this paper shows how the mean annual water balance of each catchment deviates from the asymptotes in the Budyko framework by the impacts of mean climate, soil water storage capacity as well as different climate variabilities. A conceptual hydrological model is developed in this paper for quantifying the contributions of different climate variabilities by comparing runoff resulting from different timescale climate inputs. This paper is organized as follows: In Section 2, the conceptual water balance model is presented, followed by how to apply different timescale climate inputs in the daily water balance model, and lastly, the methods for quantifying the roles of different climate variabilities on runoff at the four timescales. Results and discussion are presented in Section 3, followed by summary in Section 4.

2. Methodology

2.1 A conceptual water balance model

It is challenging, if not impossible, to directly separate the impact of different climate variabilities on the water balance using climate and runoff observations. Hydrological models are powerful tools for evaluating and predicting the water balance under different climate conditions by changing the climate inputs. A new conceptual hydrological model is developed in this study because a conceptual water balance model is simple to setup while it incorporates important hydrological processes using semi-empirical equations with a physical basis [*Devia et al.*, 2015]. The newly developed model is a modification of the HyMOD model [*Moore*, 1985; *Chen et al.*, 2013; *Razavi and Gupta*, 2016] that runs at the daily time step. Runoff at a coarser timescale can be obtained by aggregating the daily outputs.

The model structure is a saturation excess runoff model based on the spatial distribution of the soil water storage capacity (C) proposed by *Wang* [2018]:

$$F(C) = 1 - \frac{1}{a} + \frac{C+(1-a)S_b}{a\sqrt{(C+S_b)^2-2aS_bC}} \quad (1)$$

where C is soil water storage capacity at a point and $C \geq 0$; $F(C)$ is the fraction of the catchment area for which the storage capacity is less than or equal to C; a is the shape parameter with a range of $0 < a < 2$; and S_b is the average soil water storage capacity over the catchment. Figure 1 presents the schematic description of the daily water balance model. As shown in this figure, precipitation is partitioned into soil wetting (i.e., infiltration, W) and runoff (R). Soil wetting, determined by both precipitation (P) and the initial soil water storage (S_0), is computed by the following integration [*Moore*, 1985]:

$$W = \int_{C_0}^{P+C_0}[1 - F(C)]dC \quad (2)$$

where C_0 is the point storage capacity corresponding to S_0 in Figure 1. Substituting Equation (1) into Equation (2), soil wetting is obtained:

$$W = \frac{P + S_b\sqrt{(m+1)^2 - 2am} - \sqrt{[P+(m+1)S_b]^2 - 2amS_b{}^2 - 2aS_bP}}{a} \tag{3}$$

where,

$$m = \frac{S_0(2S_b - aS_0)}{2S_b(S_b - S_0)} \tag{4}$$

If initial soil water storage is zero ($S_0 = 0$), Equation (3) becomes the proportionality relationship of the *SCS* curve number method [*SCS*, 1972; *Wang*, 2018]. Therefore, the computation of soil wetting by Equations (3) is an extension of the *SCS* curve number method by explicitly incorporating initial soil moisture.

Once soil wetting (W) is computed using Equation (3), the sum of soil wetting and initial soil water storage ($Y = W + S_0$) is then partitioned into evaporation (E) and ending soil water storage (S_1), i.e., $Y = E + S_1$. In the HyMOD model, E is assigned as the smaller value between Y and potential evapotranspiration proportional to the catchment saturation degree. Alternatively, in this model, the spatial heterogeneity of soil water storage is considered when determining evaporation. As shown in Figure 1, the actual soil water storage varies spatially due to the spatial variability of storage capacity. Therefore, the actual evaporation will also vary spatially even though the potential evapotranspiration is assumed to be spatially uniform. When the soil water storage at every element in a catchment reaches their individual storage capacities (Figure 2a) (i.e., the entire catchment is saturated), then the average evaporation over the entire catchment is computed as follows:

$$E_s = \int_0^{E_p}[1 - F(C)]dC \tag{5}$$

As presented in Figure 2a, the spatially averaged evaporation under conditions when the entire catchment is saturated (E_s) is smaller than E_p, even though the average storage (S_b) is greater than E_p. The reason is that the soil water storage at some elements in the catchment are lower than E_p and the evaporation at those points are equal to the corresponding soil water storage. For the condition when the catchment is not fully saturated (Figure 2b) with an average storage of $W + S_0$, evaporation is proportionally reduced from E_s relative to the soil water storage using Equation (6):

$$E = \frac{W+S_0}{S_b} E_s \tag{6}$$

Therefore, evaporation is computed by the following equation after substituting Equation (1) into Equation (5):

$$E = \frac{W+S_0}{S_b} \frac{E_p+S_b-\sqrt{\left(E_p+S_b\right)^2-2aS_bE_p}}{a} \tag{7}$$

In the daily water balance model, runoff is decomposed into either direct runoff (R_d) or groundwater recharge (R_g) using a partitioning parameter (γ). The direct runoff and groundwater recharge are then stored in a quick storage tank (S_d) and a slow storage tank (S_g), respectively. These tanks are conceptually lumped storages representing the surface water body (S_d) and the unsaturated zone and shallow groundwater aquifer (S_g). Because water in the storage tanks cannot be totally released to the catchment outlet within one day after precipitation, therefore, linear relationships between tank outflows and tank storages are used for the routing processes. Correspondingly, the total runoff at the catchment outlet (Q) can be calculated using Equation (8-1) through Equation (8-8):

$$R = P - W \tag{8-1}$$

$$R_d = \gamma R \tag{8-2}$$

$$R_g = (1-\gamma)R \tag{8-3}$$

$$Q_d = k_d(S_{d0} + R_d) \tag{8-4}$$

$$S_{d1} = (1-k_d)(S_{d0} + R_d) \tag{8-5}$$

$$Q_b = k_b(S_{g0} + R_g) \tag{8-6}$$

$$S_{g1} = (1 - k_b)(S_{g0} + R_g) \tag{8-7}$$

$$Q = Q_d + Q_b \tag{8-8}$$

where the reciprocals of parameters k_d and k_b are the average characteristic times of the quick storage tank and slow storage tank; Q_d and Q_b are the flow rates of direct runoff and baseflow measured at the catchment outlet; S_{d0} and S_{g0} are the initial storages in the quick storage tank and slow storage tank; S_{d1} and S_{g1} are the final storages in the quick storage tank and slow storage tank.

In total, there are five parameters for the daily model: a, S_b , γ, k_b, and k_d. The ranges and units of the parameters are shown in Table 1. Monthly and annual runoff are aggregated from the daily runoff, and the mean annual runoff is the average of annual runoff. The role of the soil water storage capacity and its spatial variability have received considerable attention in the mean annual water balance because the spatially variable storage capacity promotes the mean annual runoff generation [*Milly*, 1994]. In order to quantify the role of soil water storage capacity and its spatial variability, a base simulation scenario with a spatially uniform soil water storage capacity is developed for mean annual water balances. In this scenario, the uniform storage capacity is large enough so that no saturation excess runoff occurs, and the actual daily evaporation is calculated as the smaller value between the potential evapotranspiration proportional to the catchment saturation degree and the storage water:

$$E = \min(\frac{Y}{S_b}E_p, Y) \tag{9}$$

where, $Y = W + S_0$, is the soil water storage after infiltration.

2.2 Climate inputs to the daily water balance model

Climate data at different timescales contain different components of climate variability. Specifically, daily climate data have the information of daily, monthly, and inter-annual climate variabilities. While, monthly climate lacks the daily climate information. Similarly, inter-annual climate further lacks monthly climate information. In order to run the daily water balance model with climate data at different timescales, all the climate inputs are forced with the model at the daily time step. For instance, to force the daily model with climate data that varies inter-annually, daily climate data are averaged over each year, then that average is fixed for each day within that given year (Figure 3c). Inputs are averaged over periods corresponding to the climate timescale; shown in Figure 3 are four patterns (daily, monthly, annual, and mean) of climate inputs for Caney River in Kansas during a three-year period. Model calibration is done using observed daily precipitation and daily potential evapotranspiration (Figure 3a).

The inter-annual climate inputs at the daily time step shown in Figure 3c describe the inter-annual variability of climate forcings. Comparing results from using inter-annual climate (Figure 3c) and mean climate (Figure 3d) can show the role of inter-annual climate variability on runoff at the desired timescale. Likewise, runoff from monthly climate (Figure 3b) can be compared with runoff using annually varying climate (Figure 3c) to show the role of monthly climate variability on water balance. Lastly, daily climate (Figure 3a) can be used with monthly climate (Figure 3b) to show the role of daily climate variability on water balance. Runoff is simulated using the daily water balance model forced with each type of daily inputs shown in Figure 3, therefore, each timescale runoff has four simulated series corresponding to the four climate forcings.

2.3 Study catchments and data

Eighty-two catchments from Model Parameter Estimation Experiment (MOPEX) [*Duan et al.*, 2006] with minimum snow effects and human interferences [*Kienzle*, 2008; *Brooks et al.*, 2011; *Wang and Hejazi*, 2011] were selected for this study. Catchment area ranges from 134 to 9886 km^2 and the climate aridity index ranges from 0.27 to 1.33. The hydrologic model used in this study is most useful for catchments where the saturation excess runoff regime is dominant. Therefore, catchments with a climate aridity index larger than 1.5 were not considered in this study because infiltration excess runoff generation would be significant in these catchments. Observed daily runoff for the years 1979-2003 is obtained through the MOPEX website (https://www.nws.noaa.gov/ohd/mopex/mo_datasets.htm), and extended through 2015 using the U.S. Geological Survey's (USGS) National Water Information System (https://waterdata.usgs.gov/nwis/sw). Daily precipitation and daily reference potential evapotranspiration are extracted from a gridded surface meteorological data set (gridMET) for the years 1979-2015 with a spatial resolution of ~4 km (http://www.climatologylab.org/gridmet.html) [*Abatzoglou*, 2013]. Daily reference potential evapotranspiration in gridMET is calculated using the Penman-Monteith equation [*Monteith*, 1964; *Allen et al*, 1998; *Abatzoglou and Ficklin*, 2017]. Mean annual potential evapotranspiration values from MOPEX website are used for scaling the reference potential evapotranspiration in each study catchment.

2.4 Parameter estimation and model performance

There are five parameters (i.e., a, S_b , γ, k_b, and k_d) in the daily water balance model. The parameters are conceptual representations of catchment characteristics. Thus, it is difficult to assign values using direct observations, instead, they can be determined through calibration. Available data are divided into three periods: 1) the warm-up period (1979-1980), 2) the calibration period (1981-1998), and 3) the validation period (1999-2015). Model parameters are calibrated using a Shuffled Complex Evolution Method (SCE-UA) [*Duan et al.*, 1992] and an open source python package SPOTPY [*Houska et al.*, 2015]. The objective function (*OBJ*) consists of 6 components, including 3 Nash-Sutcliffe Efficiencies (*NSE*) [*Nash and Sutcliffe*, 1970; *Moriasi et al.*, 2007] and 3 Volumetric Fit Efficiencies (*VFE*) [*Wang et al.*, 2009] corresponding to daily, monthly, and annual runoffs, as shown:

$$OBJ = \left|1.0 - NSE_{daily}\right| + \left|1.0 - NSE_{monthly}\right| + \left|1.0 - NSE_{annual}\right| + \left|1.0 - VFE_{daily}\right| + \left|1.0 - VFE_{monthly}\right| + \left|1.0 - VFE_{annual}\right| \quad (10)$$

$$NSE_{daily} = 1 - \frac{\sum_{d=1}^{D}\left(Q_s^d - Q_o^d\right)^2}{\sum_{d=1}^{D}\left(Q_o^d - \overline{Q_{o,daily}}\right)^2} \quad (11\text{-}1)$$

$$NSE_{monthly} = 1 - \frac{\sum_{m=1}^{M}\left(Q_s^m - Q_o^m\right)^2}{\sum_{m=1}^{M}\left(Q_o^m - \overline{Q_{o,monthly}}\right)^2} \quad (11\text{-}2)$$

$$NSE_{annual} = 1 - \frac{\sum_{y=1}^{Y}\left(Q_s^y - Q_o^y\right)^2}{\sum_{y=1}^{Y}\left(Q_o^y - \overline{Q_{o,annual}}\right)^2} \quad (11\text{-}3)$$

$$VFE_{daily} = \frac{\sum_{d=1}^{D} Q_s^d}{\sum_{d=1}^{D} Q_o^d} \quad (11\text{-}4)$$

$$VFE_{monthly} = \frac{\sum_{m=1}^{M} Q_s^m}{\sum_{m=1}^{M} Q_o^m} \quad (11\text{-}5)$$

$$VFE_{annual} = \frac{\sum_{y=1}^{Y} Q_s^y}{\sum_{y=1}^{Y} Q_o^y} \quad (11\text{-}6)$$

where Q_o^d (Q_o^m, Q_o^y) is the observed daily (monthly, annual) runoff on the d^{th} day (m^{th} month, y^{th} year); Q_s^m (Q_s^m, Q_s^y) is the simulated daily (monthly, annual) runoff; $\overline{Q_{o,daily}}$ ($\overline{Q_{o,monthly}}$, $\overline{Q_{o,annual}}$) is the observed mean daily (monthly, annual) runoff during the calibration period; and D (M, Y) is the total number of days (months, years) for calibration.

Including daily, monthly, and annual runoff in the objective function for calibration ensures that the model performance is satisfactory at multiple timescales [*Schaake et al.*, 1996; *Hay et al.*, 2006; *Sudheer et al.*, 2007]. In addition, using two performance metrics in calibration, *NSE* and *VFE*, will simultaneously improve estimation of the hydrograph and of volumetric fitting. The value of *NSE* ranges from $-\infty$ to 1, with a value of 1 representing a perfect estimation of observed variability. *VFE*, ranging from $-\infty$ to ∞, reflects model bias with a value of 1 corresponding to no model bias. The same objective function weights for *NSE* and *VFE* are used for 3 timescales modeled in this study. Parameter values are chosen for each catchment by minimizing the objective function and fixing them for each model run.

2.5 Roles of climate variability on runoff at different timescales

2.5.1 Daily, monthly, and annual runoff

The role of each climate variability in daily, monthly, or annual runoff is defined as its ability to explain runoff variability at each timescale. This ability is quantified by the difference in *NSE* values from the simulated runoff using the climate inputs at two consecutive timescales. Quantifying the role of climate variability in this study uses *NSE* because it is an indicator for evaluating the overall model behavior with an emphasis on the timing and shape of the hydrograph which reflects the sensitivity of runoff to climate fluctuations. Additionally, *NSE* can be applied to runoff at different timescales. A consistent index across timescales helps systematically compare the roles of each climate variability on runoff at multiple timescales. The role of each climate variability in terms of ΔNSE is normalized by the *NSE* value resulting from daily climate, shown in the following equation:

$$\rho_{i,j} = \frac{NSE_{i,j} - NSE_{i+1,j}}{NSE_{1,j}} \qquad (12)$$

where $\rho_{i,j}$ represents the relative role of the i^{th} (i = 1, 2, 3) timescale climate variability on the j^{th} (j = 1, 2, 3) timescale runoff. For example, Figure 4a shows the flow chart for quantifying the roles of different climate variabilities (i = 1 for daily climate variability, i = 2 for monthly climate variability, and i = 3 for inter-annual climate variability) on the daily runoff (j = 1). The role of daily climate variability on the daily runoff is quantified as the difference in *NSE* from the model driven by daily climate (e.g., Figure 3a) and by monthly climate (e.g., Figure 3b), i.e., $NSE_{1,1} - NSE_{2,1}$. The role of monthly climate variability on daily runoff is quantified as the difference in *NSE* from the model driven by monthly climate (Figure 3b) and by inter-annual climate (Figure 3c), i.e., $NSE_{2,1} - NSE_{3,1}$. Likewise, the role of inter-annual climate variability on the daily runoff variability is quantified as the difference in *NSE* driven by inter-annual climate (Figure 3c) and by mean climate (Figure 3d), i.e., $NSE_{3,1} - NSE_{4,1}$. Note that, since $NSE_{4,j}$ represents the performance of the model forced with the mean annual climate, the model runoff will approach the observed long-term mean causing the *NSE* to be very close to zero. Recall, a value of "0" for *NSE* means that a model can only simulate the mean of the observed data. Similarly, the roles of the climate variabilities at the three timescales on monthly runoff (j = 2), and annual runoff (j = 3) are quantified based on Equation (12).

2.5.2 Mean annual water balance

Following *Milly* [1994], the roles of climate variabilities on the mean annual water balance are defined as their contributions to the total runoff generation and are quantified through the runoff differences with different forcing inputs. In addition to the climate variability, the roles of the long-term mean climate and soil water storage capacity with its spatial variability are evaluated for the mean annual water balance in order to compare to the results of other studies. The total mean annual runoff in each catchment is decomposed into 5 components, as follows:

$$Q_{total} = Q_D + Q_M + Q_I + Q_S + Q_L \tag{13}$$

$$Q_D = Q_1 - Q_2 \tag{14-1}$$

$$Q_M = Q_2 - Q_3 \tag{14-2}$$

$$Q_I = Q_3 - Q_4 \tag{14-3}$$

$$Q_S = Q_4 - Q_5 \tag{14-4}$$

$$Q_L = Q_5 \tag{14-5}$$

where Q_1 (=Q_{total}), Q_2, Q_3, and Q_4 are the simulated mean annual runoffs forced by daily climate (Figure 3a), monthly climate (Figure 3b), inter-annual climate (Figure 3c), and long-term mean climate (Figure 3d), respectively. Q_1 ~ Q_4 are the simulated runoffs from the water balance model with spatially variable storage capacity. Q_5 (or Q_L) is the simulated runoff forced by mean climate without considering the spatial variability of soil water storage capacity and having a uniformly distributed storage capacity that is large enough so that no saturation excess runoff occurs. Therefore, Q_D , Q_M, Q_I, Q_S, Q_L are the 5 components of the total mean annual runoff, which are caused by daily climate variability, monthly climate variability, inter-annual climate variability, storage capacity with its spatial variability, and long-term mean climate, respectively. The contribution of each component is normalized by the total mean annual runoff:

$$\rho_{component} = \frac{Q_{component}}{Q_{total}} \tag{15}$$

where $Q_{component}$ represents the components of total runoff as mentioned in Equation (13); $\rho_{component}$ represents the relative role of each component on mean annual runoff. The decomposition process and the role quantification process for the mean annual runoff are shown in Figure 4b.

3. Results and discussion

3.1 Model performance

The calibrated parameters for 12 catchments (locations shown in Figure 10) are listed in Table 1. Values of the shape parameter (a) for these catchments are close to the upper limit (i.e., 2). Considering all catchments used in the study, the shape parameter values ranges from 1.85 to 1.90 for 4 catchments, with the remaining catchments having a value greater than 1.90, indicating an "S" shape of the cumulative distribution function (CDF) for soil water storage capacity [*Wang*, 2018]. The "S" shape of a CDF curve consists of both a convex and a concave segment, which introduces more flexibility for simulating runoff generation under different wetness conditions [*Jayawardena and Zhou*, 2000].

The *NSE* values for the daily, monthly, and annual runoffs during calibration and validation periods are shown in Figure 5a and Figure 5b. Generally, *NSE* is greater at coarser timescales. The average *NSE* during the calibration (validation) period is 0.61 (0.61), 0.85 (0.83), 0.90 (0.85) for the daily, monthly, and annual runoff, respectively. During validation, 52% of catchments have an *NSE* value greater than 0.6 for daily runoff, 77% of catchments have an *NSE* value greater than 0.8 for monthly runoff, and 61% of catchments have an *NSE* value greater than 0.85 for annual runoff. A comparison between the observed mean annual runoff and simulation is presented in Figure 5c for all study catchments. The relative error for the validation period is 5.9% on average, and the root mean square error is 33.0 mm/year.

The percent bias (*PBIAS*) is calculated as well for evaluating the model performance. It is expected that the *PBIAS* will be small in all catchments during calibration period because the volumetric fit efficiency (*VFE*) effectively controls the model bias and it accounts for 50% of the weight in the objective function for calibration. Results show that the average *PBIAS* during the calibration period is -0.13%. Only 5 catchments have an absolute value of *PBIAS* between 0.5% and 5%, with all other catchments having an absolute value of *PBIAS* smaller than 0.5%. The cumulative probability of the *PBIAS* during validation is shown in Figure 5d. The *PBIAS* during validation is larger compared to that during calibration, while still acceptable, the average *PBIAS* is -0.28% for all the catchments. Eight-seven percent of the catchments have a *PBIAS* within ±10%, indicating that no significant bias exists in the model [*Moriasi et al.*, 2007; *Gupta et al.*, 2009]. The relatively larger model bias during the validation period in this study probably is ascribed to the decreasing runoff ratio (the ratio between mean annual runoff and mean annual precipitation) in most of the catchments, even though the catchments selected in this study are relatively less influenced by climate change and human activities compared to other MOPEX catchments. As for the 11 catchments with a bias larger than 10% during the validation period, the runoff ratio is changed by 16.3% on average, which is higher than that from the other catchments (9.5%). Note that the model performance is not dependent on the catchment drainage area (see Figure S1 in the Supporting Information).

The model performance is satisfactory for the daily, monthly, annual, and mean annual water balance considering its parsimonious model structure [*Perrin et al.*, 2001; *McIntyre et al.*, 2005; *Moriasi et al.*, 2007; *Wang et al.*, 2009]. To compare the model performance with other models, HyMOD [*Moore*, 1985] was used for all study catchments. The performance of the two models are shown in Figure S2 of the Supporting Information. The comparison shows that our model is superior to HyMOD in simulating the daily and monthly runoff, and has a similar efficiency in simulating the annual runoff. The average bias in simulating runoffs using the new conceptual model is smaller than the bias from HyMOD. Note that in the Supporting Information, the model used in this study is referred to as PDM-CN model for simplification since our model is a probability distributed model (PDM), and the distribution function for soil water storage capacity used in this model leads to the SCS-CN method [*Wang*, 2018].

3.2 The roles of climate variabilities on runoff

The relative roles of different climate variabilities on the runoff at different timescales for the 82 study catchments are presented in Figure 6. In the daily runoff, the average relative role of daily variability is the largest, accounting for 50.2% of the daily runoff variability (Figure 6a). Monthly climate variability has the second most contribution, explaining 40.9% of the daily runoff variability (Figure 6a). The relative role of inter-annual variability is much smaller, only explaining 8.9% of the daily runoff variation. The dominant contribution of the erratic rain pattern of storminess calls for daily climatic data when simulating daily runoff. However, daily data are not fully accessible in many catchments, therefore, making it difficult to accurately simulate the daily runoff. Additionally, the high contribution of the monthly variability indicates strongly monthly characteristics in daily rainfall events and significant storage variation at the daily scale resulting from the monthly climatic fluctuations. Flashiness is one of the most marked characteristics of daily runoff, thus the Richards-Baker flashiness index (*R-B* Index) [*Baker et al.*, 2004] is calculated for daily runoff during the validation period (1999-2015) to further present the sensitivity of daily runoff to different climate variabilities. Runoff with a larger *R-B* Index experiences a larger day-to-day variation. The results show that the *R-B* Index for the simulated runoff with daily climate input is 0.25 on average among the study catchments, and is reduced to 0.02 when using monthly climate input. There is almost no flashiness in the simulated runoff when inter-annual climate is used, and there is no flashiness in runoff using mean climate since the catchment reaches a steady state. Figure 7a shows a three-year daily runoff hydrograph with different climate inputs for Smith River in California (USGS gage number: 11532500). The remarkable difference in flashiness of the simulated runoff modeled with different climate inputs further manifests the essential role played by daily climate variability on daily runoff. Additionally, monthly climate variability generally determines the shape of daily runoff at the monthly scale, and it is also a key component for daily runoff variation.

In the monthly water balance, the role of monthly climate variability is the largest, on average explaining 75.5% of the variation in monthly runoff (Figure 6b). The roles of daily and inter-annual climate variability are much smaller, contributing 6.9% and 17.6% of the monthly runoff variation, respectively. The central role of monthly climate variability on the monthly water balance is also supported by the Pardé coefficient, which is an indicator for identifying the mean seasonal flow regime [*Pardé*, 1933]. Figure 7b shows the distribution of the Pardé coefficient for Smith River. The runoff seasonality is almost fully determined by the monthly climate variability since other climate variabilities explain less variation in monthly runoff. The overwhelming control of the monthly climate variability on the monthly runoff variability reduces the difficulty in model prediction compared to the daily timescale because monthly climatic data are more accessible. The much smaller role of the daily variability indicates that the irregular effects of daily storminess are smoothed out at the monthly scale by the soil water storage capacity. This is supported by *Wang et al.* [2011] which found that the daily forcings did not improve the performance of the monthly water balance much, through comparing a monthly water balance model with two daily water balance models in simulating the monthly runoff. Figure 8a shows the relative role of monthly climate variability on monthly runoff variation as a function of climate aridity index. In wetter areas, more variance in monthly runoff could be explained by the monthly climate variability than in drier areas. However, the monthly climate variability still explains more than half of the variation in monthly runoff for drier catchments.

In the annual water balance, the inter-annual climate variability explains the most variation (81.5% on average) in the inter-annual runoff (Figure 6c). The monthly climate variability also has a considerably contribution (17.4%). However, the impacts of daily variability are further diluted in the annual runoff compared to that in the monthly runoff. Figure 7c shows the simulated annual runoff in Smith River with different climate inputs. The power of inter-annual climate variability over annual runoff can also be reflected by the coefficient of variation (*CV*) of simulated annual runoff. The *CV* value increases from 0, when using mean climate, to 0.0155 using annually variable climate and does not change much with smaller timescale climate inputs indicated by Figure 7c. Figure 8b shows that the relative contribution of inter-annual climate variability on the annual runoff variation is larger in wetter catchments than in drier catchments. In some humid catchments, the contribution of the inter-annual variability is up to 100%. Figure 8c shows a positive relationship between the relative role of monthly climate variability on the annual runoff and the climate aridity index. Therefore, the impact of monthly variability is larger in drier regions. This result generally agrees with the result from *Milly and Dune* [2002], which found that the inter-annual variance in runoff was explained more by annual climate anomalies than by seasonality, especially in humid catchments. Figure 8b and 8c show the significant controls of the mean annual climate (in terms of climate aridity index) on the relative sensitivity of annual runoff to different climate variabilities. The large scatter in Figure 8b-c indicates that other catchment characteristics also have contribution in determining the relative role of climate variability. Figure 8d shows the relationship between the total contribution of climate variability on the annual runoff and climate aridity index with colors indicating base flow indexes. The base flow index is estimated by base flow separation using a recursive digital filter based on *Eckhardt* [2005]. The total contribution of climate variability in each catchment is computed as the standard deviation of ΔQ normalized by ΔP in annual time series, where ΔQ is the difference between the runoff using mean annual climate (Figure 3d) and runoff using daily climate (Figure 3a). Since the initial condition and the total annual precipitation depth are same for the different climate patterns (e.g., Figure 3a and Figure 3d), the runoff difference is caused by climate variabilities, including the daily, monthly, and inter-annual variability. As shown in Figure 8d, the catchments within the red dashed rectangle have a relatively larger base flow index. This suggests that catchments experiencing the same climate regime, and a larger base flow index will tend to receive less impacts from climate variations due to the filtering effect of groundwater. Groundwater has a longer residence time than surface water and diminishes the effects of climate variation observed in runoff. The buffering effects of groundwater against climate fluctuations in the study catchments are not as strong as that in the semi-arid catchments, seen in *Istanbulluoglu et al.* [2012]. The relative smaller effect of groundwater on the runoff resilience in the study catchments is further indicated by a weak relation between the base flow index and the Hurst exponent (*H*), an indicator for the long-term memory of runoff [*Hurst*, 1951], as shown in Figure 8d-1. A runoff time series with $H = 0.5$ is known as a Brownian time series (i.e., there is no autocorrelation), a range of $0.5 < H \leq 1$

suggests a long-term memory of runoff, and $H < 0.5$ suggests an anti-persistent time series [*Hurst*, 1951]. The points in Figure 8d-1 and 8d-2 are catchments within the range $0.5 < H \leq 1$. Compared to Figure 8d-1, a stronger relationship between the annual precipitation Hurst exponent and the annual runoff Hurst exponent is found in Figure 8d-2, implying a stronger dependence between precipitation and runoff variation in the study catchments.

Figure 6d shows the relative roles of each climate variability on the mean annual runoff. Note that the values in Figure 6d are not supposed to be compared with values of relative roles from the water balances at smaller timescales (Figure 6a-c), because the method to calculate the relative roles of climate variability on the mean annual runoff is different. Among different climate variabilities, monthly climate variability is the most important, contributing 64.7%, on average, to the part of mean annual runoff that generated by climate variabilities. It should be pointed out that the inter-annual climate variability also plays a substantial role in the mean annual runoff, contributing 22.2%, on average, to the climate variability-generated mean annual runoff. This result supports a previous research in *Li* [2014], which showed that the inter-annual variability of precipitation and potential evapotranspiration reduces the mean annual evapotranspiration based on a stochastic soil moisture model. The reduction in evaporation ratio can reach 8-10% for the range of precipitation and potential evapotranspiration variability used in the study, which means that the inter-annual climate variability promotes the runoff generation.

Figure 6 shows that at the daily, monthly, and annual timescales, the variation in runoff is largely determined by the climate variability at the same temporal scale. Specifically, for the annual runoff, the inter-annual variability plays the most important role, and so on. Following this pattern, the long-term climate condition (in terms of climate aridity index) should be most important for the long-term mean annual water balance; this claim has been widely confirmed in other studies [*Budyko*, 1958, 1974; *Milly*, 1994; *Zhang et al.*, 2001; *Yang et al.*, 2008; Gentine *et al.*, 2012].

The relative roles of climate variability have also been evaluated based on simulation results from HyMOD. The results from the model developed in this paper and that based on HyMOD are summarized in Table S1 and S2, respectively. It shows that the results from these two models are consistent. It is possible that a different combination of weights in the objective function could lead to different model efficiency. However, the relative contribution of each climate variability is normalized by the model behavior from the daily climate as shown in Equations (12) and (15), which suggests an insensitivity of the relative effects of climate variability to the weights used in calibration. Moreover, Table S3 in the Supporting Information shows the results of the relative roles of climate variability based on the simulation results with the parameters calibrated by *NSE* only (not using *VFE*). As shown in Table S1 and Table S3, no noticeable difference is observed between the results from the two calibration objective functions (i.e., *NSE* and *VFE* versus *NSE* only).

3.3 Budyko framework

In addition to the climate variability, the direct contributions of the mean climate and soil water storage capacity are also evaluated in the mean annual water balance (Figure 9). Among all the factors, the mean climate is the dominant factor controlling the precipitation partitioning, contributing 57.6 %, on average, to the mean annual runoff. The soil water storage capacity with its spatial variability is the second contributing factor and contributes on average 30.3% of the mean annual runoff. The spatial heterogeneity of soil water storage not only promotes the runoff generation directly but also suppresses the evaporation over the catchment as shown in Figure 2.

The impact of daily storminess on the mean annual water balance is small for the study catchments. This result is similar to *Reggiani* [2000] who found that the storminess has an almost negligible effect on the mean annual water balance when infiltration excess runoff is negligible.

Figure 10 shows how the mean annual evaporation ratio (i.e., $\frac{E}{P}$) for the 12 catchments in Table 1 deviates from the asymptotes in the Budyko framework. Each data point in Figure 10 (except for the observation) is a simulated evaporation ratio using the indicated forcing for each catchment. When neglecting climate variability and soil water storage capacity as well as its spatial heterogeneity, the mean annual evaporation of a catchment is the highest (red circles), falling on the asymptotes (dashed black lines). In a catchment with a climate aridity index smaller than 1, the evaporation is equal to the potential evapotranspiration. Conversely, a catchment with a climate aridity index larger than 1, the evaporation is equal to precipitation. A horizontal line with $\frac{E}{P} = 1$, is referred to as the upper bound in this paper (dashed dotted red line) which is not possible exceeded at the mean annual scale because of mass balance principle. The deviation from the upper bound (dashed dotted red line) to the asymptotes (dashed black lines) could be interpreted as the direct contribution of mean climate to mean annual runoff. This deviation decreases to 0 when the aridity index is greater than 1. It suggests that the mean climate has direct contribution to mean annual runoff only in catchments with a climate aridity index less than 1, although the mean climate can play roles in runoff generation in drier areas through the coevolution with other catchment properties such as the soil water storage capacity and vegetation. Soil water storage capacity and climate variability promote runoff generation, therefore, the evaporation ratio further deviates from the asymptotes when more factors are considered and eventually approaches the observed value when all factors are considered [*Milly*, 1994; *Westhoff et al*., 2016].

The contribution of each catchment characteristic to the mean annual runoff versus climate aridity index ($\frac{E_p}{P}$) is shown in Figure 11. It is apparent that the direct contribution of mean climate decreases with climate aridity index and is 0 for catchments when the climate aridity index is equal to or larger than 1 (Figure 11a). Other catchment characteristics including the storage capacity interact with the local climate, therefore, a clear pattern would also be found between the relative role of the spatially variable storage capacity with the climate aridity index (Figure 11b). The contributions of storage capacity and climate variabilities increase as climate becomes drier (Figure 11b, c, d). The scatter in Figure 11 suggests that the contribution of each component is not only dependent on the mean annual climate but also other unconsidered factors (e.g., sub-daily rainfall variability and topography).

3.4 A unified framework for water balance models

The developed daily water balance model provides a unified framework for modeling runoff at different timescales. For the traditional daily, monthly, annual, and long-term water balance models, the timescale of climate inputs is same as that of runoff to be modelled (Figure 12). For example, monthly water balance models [*Thomas*, 1981; *Makhlouf and Michel*, 1994] take monthly precipitation and potential evapotranspiration as the inputs as shown in Figure 12-b1. Model complexity and parameter uncertainty is a trade-off during model development [*Perrin et al.*, 2001; *Zhang et al.*, 2008]. Generally, as the model timescale becomes coarser, the model performance is not sacrificed in return for simpler model complexity [*Jothityangkoon et al.*, 2001]. But the model complexity as well as the number of parameters should be flexible in different catchments and based on different research purposes. Assuming the residence time for the quick storage tank is much less than one month, the monthly water balance model is obtained by removing the routing of quick storage as shown in Figure 12-b2 (i.e., k_d=1 in Equations 8-4 and 8-5) and the equations for the remaining components are same as those of daily water balance model. The monthly water balance model shown in Figure 12-b2 has a similar performance as the 'abcd' model (see Figure S3 in Supporting Information), which is a state-of-the-art monthly water balance model with 4 parameters [*Thomas*, 1981]. In Equation (3), precipitation is partitioned into soil wetting and runoff; whereas, in the 'abcd' model, the sum of precipitation and initial storage is partitioned into runoff and the sum of ending storage and evaporation. However, Equation (3) with $S_0 = 0$ leads to the same functional form as the 'abcd' model for calculating runoff. Assuming that the residence time for the slow storage tank is less than one year, the routing of slow storage could be removed, resulting in the two-parameter (a, S_b) annual model as shown in Figure 12-c2 (i.e., k_d =1 in Equations 8-4 and 8-5, and k_b=1 in Equations 8-6 and 8-7). Driven by annual precipitation and potential evapotranspiration (Figure 12-c1), the annual water balance model calculates annual soil wetting (and runoff as $P - W$) by Equation (3) and annual evaporation by Equation (7). The soil water storage carryover in the annual water balance model is considered through the initial storage in Equation (3).

Since soil water storage carry-over is not necessary for long-term water balances, the mean annual water balance model is obtained by removing the initial soil water storage (i.e., $S_0 = 0$) as shown in Figure 12-d2. Equation (3) becomes:

$$W = \frac{P+S_b-\sqrt{(P+S_b)^2-2aS_bP}}{a} \tag{16}$$

Dividing by P on both sides of the equation, Equation (16) leads to a one-parameter Budyko-type equation [*Wang and Tang*, 2014]. Substituting Equation (16) into Equation (7) and dividing P on both hand sides, one obtains:

$$\frac{E}{P} = \frac{\Phi^{-1}+1-\sqrt{(\Phi^{-1}+1)^2-2a\Phi^{-1}}}{a} \cdot \frac{\frac{E_p}{P}+\Phi-\sqrt{\left(\frac{E_p}{P}+\Phi\right)^2-2a\Phi\frac{E_p}{P}}}{a} \tag{17}$$

where $\Phi = \frac{S_b}{P}$ is soil storage index. Equation (17) shows that $\frac{E}{P}$ is a function of $\frac{E_p}{P}$, Φ, and a. This mean annual water balance model can be interpreted as the two-stage precipitation partitioning [*L'vovich*, 1979]. At the first stage, a portion of precipitation is partitioned to soil wetting; at the second stage, a portion of soil wetting is partitioned into evaporation. If all the precipitation becomes soil wetting at the first stage (i.e., $P = W$), the two-stage partitioning is simplified as a one-stage partitioning (i.e., precipitation is partitioned into evaporation and runoff directly). For the one-stage partitioning, the available water for evaporation is precipitation, and the average soil water storage capacity (i.e., S_b) in Figure 12-d2 is set as P. Correspondingly, Equation (7) becomes the one-parameter Budyko equation [*Wang and Tang*, 2014]:

$$\frac{E}{P} = \frac{\frac{E_p}{P}+1-\sqrt{\left(\frac{E_p}{P}+1\right)^2-2a\frac{E_p}{P}}}{a} \tag{18}$$

The five-parameter daily water balance model (Figure 12-a), which unifies the probability distributed model and the SCS-CN method [*Wang*, 2018], can be easily modified to a coarser modeling timescale by removing unnecessary components (Figures 12-b, 12-c, and 12-d). The equations for the common components among different timescale models remain the same. The four-parameter monthly model (Figure 12-b) is obtained by removing the routing of quick flow; and the two-parameter annual model (Figure 12-c) is obtained by further removing the routing of slow flow; and the two-parameter mean annual model (Figure 12-c) is obtained by neglecting initial storage (Equation 17) in the annual model. The two-parameter mean annual model can be further simplified as a one-parameter Budyko model (Equation 18). However, the HyMOD cannot lead to the Budyko model by the same simplification. It should be noted that the common parameters (e.g., a) among the different timescale models (Figure 12) have different values due to the timescale effect [*Deng et al.*, 2018]. To avoid the effect of climate timescale on model parameters, precipitation and potential evapotranspiration at the daily time step (Figure 3) can be used for modelling runoff at different timescales. In this case, the common parameters for modeling runoff at different timescales have the identical values.

4. Conclusion

A new conceptual hydrological model was developed based on a new distribution function for describing the spatial variability of soil water storage capacity which leads to the SCS curve number method. In this study, the spatial variability of the soil water storage was assumed to have impacts on both runoff generation and evaporation. Parameters (5 in total) were calibrated using the SCE-UA algorithm with the objective function being the weighted combination of Nash-Sutcliffe efficiencies and volumetric fit efficiencies from daily, monthly, and annual runoff. The relative effects of climate variabilities (i.e., temporal variabilities of precipitation and potential evapotranspiration), on the runoff at different timescales were evaluated by comparing the simulated runoff with different timescale climate data. The results show that at the daily, monthly, and annual scales, runoff variation is mostly influenced by the climate variability at the same timescale. As for the mean annual runoff, monthly climate variability is the predominant contributor among all the climate variabilities, and our study confirms that inter-annual climate variability affects the mean annual runoff considerably. The roles of the mean climate and soil water storage capacity with its spatial variability were also quantified for the mean annual runoff. The mean climate is the direct contributor to mean annual runoff only in humid catchments. The soil water storage capacity and climate variabilities play more important roles in contributing the mean annual runoff in drier regions. The daily water balance model built in this study provides a unified framework which unifies water balances at different timescales.

It should be noted that this study only tried to investigate the relative roles of different climate variabilities in a broader sense, while other catchment characteristics are not explored thoroughly but are also important to the water balance. This study helps gain insight into the general control of the climatic fluctuations on the water balance. While, the results from this paper are more applicable to humid catchments since the model developed is a saturation excess model. Infiltration excess runoff regime will be incorporated in future research.

Acknowledgements

This research was funded in part under award CBET-1804770 from National Science Foundation (NSF) and United States Geological Survey (USGS) Powell Center Working Group Project "A global synthesis of land-surface fluxes under natural and human-altered watersheds using the Budyko framework". The dataset and computer code used to complete the analysis in this paper can be downloaded from http://www.hydroshare.org/resource/dae72cfc4f7d41028b0ab8864b17fedd.

References

Abatzoglou, J. T. (2013), Development of gridded surface meteorological data for ecological applications and modelling, *Int. J. Climatol.*, *33*, 121-131.

Abatzoglou, J. T., and D. L Ficklin (2017), Climatic and physiographic controls of spatial variability in surface water balance over the contiguous United States using the Budyko relationship, *Water Resour. Res.*, *53*(9), 7630-7643.

Allen, R. G., L. S. Pereira, D. Raes, and M. Smith (1998), Crop evapotranspiration-Guidelines for computing crop water requirements-FAO Irrigation and drainage paper 56, FAO Rome, 300, D05109.

Appels, W. M., P. W. Bogaart, and S. E. A. T. M. van der Zee (2017), Feedbacks between shallow groundwater dynamics and surface topography on runoff generation in flat fields, *Water Resour. Res.*, *53*, 10, 336-10, 353, doi:10.1002/2017WR020727.

Arora, V. K. (2002), The use of the aridity index to assess climate change effect on annual runoff, *J. Hydrol.*, *265*(1-4), 164-177.

Atkinson, S. E., R. A. Woods, and M. Sivapalan (2002), Climate and landscape controls on water balance model complexity over changing timescales, *Water Resour. Res.*, *38*(12), 1314, doi:10.1029/2002WR001487.

Aubert, D., C. Loumagne, and L. Oudin (2003), Sequential assimilation of soil moisture and streamflow data in a conceptual rainfall-runoff model, *J. Hydrol.*, *28*0(1-4), 145-161.

Baker, D. B., P. Richards, T. T. Loftus, and J. W. Kramer (2004), A new flashiness index: Characteristics and applications to Midwestern rivers and streams, *J. Am. Water Resour. Assoc.*, *40*, 503-522.

Berghuijs, W. R., M. Sivapalan, R. A. Woods, and H. H. G. Savenije (2014), Patterns of similarity of seasonal water balances: A window into streamflow variability over a range of time scales, *Water Resour. Res.*, *50*, 5638-5661, doi:10.1002/2014WR015692.

Berghuijs, W. R., A. Hartmann, and R. A. Woods (2016), Streamflow sensitivity to water storage changes across Europe, *Geophys. Res. Lett.*, *43*, 1980-1987, doi:10.1002/2016GL067927.

Botter, G., A. Porporato, I. Rodriguez-Iturbe, and A. Rinaldo (2007), Basin-scale soil moisture dynamics and the probabilistic characterization of carrier hydrologic flows: Slow, leaching-prone components of the hydrologic response, *Water Resour. Res.*, *43*, W02417, doi:10.1029/2006WR005043.

Brooks, P. D., P. A. Troch, M. Durcik, E. Gallo, and M. Schlegel (2011), Quantifying regional scale ecosystem response to changes in precipitation: Not all rain is created equal, *Water Resour. Res.*, 47, W00J08, doi:10.1029/2010WR009762.

Brutsaert, W. (2005), *Hydrology: an introduction*, 305-365pp., Cambridge University Press, New York.

Budyko, M. I. (1958), *The Heat Balance of the Earth's Surface*, US Dep. Of Commer., Washington, D. C.

Budyko, M. I. (1974), *Climate and Life*, 508 pp., Academic Press, New York.

Deng, C., P. Liu, D. Wang, and W. Wang (2018), Temporal variation and scaling of parameters for a monthly hydrologic model, *J. Hydrol.*, 558, 290-300.

Devia, G. K., B. P. Ganasri, and G. S. Dwarakish (2015), A review on hydrological models, *Aquat. Proc*, *4*, 1001-1007.

Dettinger, M. D., and H. F. Diaz (2000), Global characteristics of stream flow seasonality and variability, *J. Hydrometeoro*, *1*(4), 289-310.

Chen, H., D. Yang, Y. Hong, J .J. Gourley, and Y. Zhang (2013), Hydrological data assimilation with the Ensemble Square-Root-Filter: Use of streamflow observations to update model states for real-time flash flood forecasting, *Adv. Water Resour.*, *59*, 209-220, doi:10.1016/j.advwatres.2013.06.010.

Chen, X., N. Alimohammadi, and D. Wang (2013), Modeling interannual variability of seasonal evaporation and storage change based on the extended Budyko framework, *Water Resour. Res.*, *49*, 6067-6078, doi:10.1002/wrcr.20493.

Donohue, R. J., M. L. Roderick, and T. R. McVicar (2007), On the importance of including vegetation dynamics in Budyko's hydrological model, *Hydrol. Earth Syst. Sci.*, *11*, 983-995.

Duan, Q., S. Sorooshian, and V. Gupta (1992), Effective and efficient global optimization for conceptual rainfall-runoff models, *Water Resour. Res.*, *28*(4), 1015-1031.

Duan, Q., J. Schaake, V. Andreassian, S. Franks, et al. (2006), Model Parameter Estimation Experiment (MOPEX): An overview of science strategy and major results from the second and third workshops, *J. Hydrol.*, *320*(1-2), 3-17, doi:10.1016/j.jhydrol.2005.07.031.

Eagleson, P. (1978), Climate, Soil, and Vegetation 2. The Distribution of Annual Precipitation Derived From Observed Storm Sequences, *Water Resour. Res.*, *14*(5), 713-721, doi:10.1029/WR014i005p00713.

Eckhardt, K. (2005), How to construct recursive digital filters for baseflow separation, *Hydrol. Processes*, *19*(2), 507-515, doi:10.1002/hyp.5675.

Fan, Y., G. Miguez-Macho, C. P. Weaver, R. Walko, and A. Robock (2007), Incorporating water table dynamics in climate modeling: 1. Water table observations and equilibrium water table simulations, *J. Geophys. Res.*, *112*, D10125, doi:10.1029/2006JD008111.

Farmer, D., M. Sivapalan, and C. Jothityangkoon (2003), Climate, soil, and vegetation controls upon the variability of water balance in temperate and semiarid landscapes: Downward approach to water balance analysis, *Water Resour. Res.*, *39*(2), 1035, doi:10.1029/2001WR000328.

Feng, X., G. Vico, and A. Porporato (2012), On the effects of seasonality on soil water balance and plant growth, *Water Resour. Res.*, *48*, W05543, doi:10.1029/2011WR011263.

Fu, B. P. (1981), On the calculation of the evaporation from land surface [in Chinese], *Chin. J. Atmos. Sci.*, *5*, 23-31.

Gentine, P., P. D'Odorico, B. R. Lintner, G. Sivandran, and G. Salvucci (2012), Interdependence of climate, soil, and vegetation as constrained by the Budyko curve, *Geophys. Res. Lett.*, *39*, L19404, doi:10.1029/2012GL053492.

Gupta, H. V., H. Kling, K. K. Yilmaz, and G. F. Martinez (2009), Decomposition of the mean squared error and NSE performance criteria: Implications for improving hydrological modelling, J. *Hydrol.*, *377*, 80-91, doi:10.1016/j.jhydrol.2009.08.003.

Hay, L. E., G. H. Leavesley, M. P. Clark, S. L. Markstrom, R. J. Viger, and M. Umemoto (2006), Step wise, multiple objective calibration of a hydro-logic model for a snowmelt dominated basin, *J. Am. Water Resour. Assoc.*, *42*(4), 877-890, doi:10.1111/j.1752-1688.2006.tb04501.x.

Han, P. F., X. S. Wang, and E. Istanbulluoglu (2018), A Null-parameter formula of storage-evapotranspiration relationship at catchment scale and its application for a new hydrological model, *J. Geophys. Res.*, *123*(4), 2082-2097

Hickel, K., and L. Zhang (2006), Estimating the impact of rainfall seasonality on mean annual water balance using a top-down approach, *J. Hydrol.*, *331*(3-4), 409-424.

Houska, T., P. Kraft, A. Chamorro-Chavez, and L. Breuer (2015), SPOTting model parameters using a ready-made python package, *PloS One*, *10*(12), e0145180, doi:10.1371/journal.pone.0145180.

Hurst, H. E. (1951), Long-term storage capacity of reservoirs, *Trans. Am. Soc. Civ. Eng.*, *116*, 770-799.

Istanbulluoglu, E., T. Wang, O. M. Wright, and J. D. Lenters (2012), Interpretation of hydrologic trends from a water balance perspective: The role of groundwater storage in the Budyko hypothesis, *Water Resour. Res.*, *48*(3), W00H16, doi:10.1029/2010WR010100.

Jayawardena, A. W., and M. C. Zhou (2000), A modified spatial soil moisture storage capacity distribution curve for the Xinanjiang model, *J. Hydrol*., *227*, 93-113.

Jasechko, S., S. J. Birks, T. Gleeson, Y. Wada, P. J. Fawcett, Z. D. Sharp, J. J. McDonnell, and J. M. Welker (2014), The pronounced seasonality of global groundwater recharge, *Water Resour. Res.*, *50*, 8845-8867, doi:10.1002/2014WR015809.

Jothityangkoon, C., M. Sivapalan, and D. L. Farmer, (2001), Process controls of water balance variability in a large semi-arid catchment: downward approach to hydrological model development, *J. Hydrol.*, *254*(1-4), 174-198.

Jothityangkoon, C., and M. Sivapalan (2009), Framework for exploration of climatic and landscape controls on catchment water balance, with emphasis on inter-annual variability, *J. Hydrol*, *371*(1-4), 154-168.

Kienzle, S. W. (2008), A new temperature based method to separate rain and snow, *Hydrol. Processes*, *22*(26), 5067-5085.

Kollat, J. B., P. M. Reed, and T. Wagener (2012), When are multiobjective calibration trade-offs in hydrologic models meaningful?, *Water Resour. Res.*, *48*, W03520, doi:10.1029/2011WR011534.

Koster, R. D., and M. J. Suarez (1999), A simple framework for examining the interannual variability of land surface moisture fluxes, *J. Clim.*, *12*, 1911-1917.

L'vovich, M. I. (1979), *World Water Resources and Their Future*, 415 pp., AGU, Washington, D. C.

Li, D., M. Pan, Z. Cong, L. Zhang, and E. Wood (2013), Vegetation control on water and energy balance within the Budyko framework, *Water Resour. Res.*, *49*, 969-976, doi:10.1002/wrcr.20107.

Li, D. (2014), Assessing the impact of interannual variability of precipitation and potential evaporation on evapotranspiration, *Adv. Water Resour.*, *70*, 1-11.

Makhlouf, Z., and C. Michel (1994), A two-parameter monthly water balance model for French watersheds, *J. Hydrol*., 162, 299-318, doi:10.1016/0022-1694(94)90233-X.

McIntyre, N., H. Lee, H. Wheater, A. Young, and T. Wagener (2005), Ensemble predictions of runoff in ungauged catchments, *Water Resour. Res.*, *41*, W12434, doi:10.1029/2005WR004289.

McMillan, H. K., and M. Srinivasan (2015), Characteristics and controls of variability in soil moisture and groundwater in a headwater catchment, *Hydrol. Earth Syst. Sci.*, *19*(4), 1767-1786, doi:10.5194/hess-19-1767-2015.

McNamara, J. P., D. Tetzlaff, K. Bishop, C. Soulsby, M. Seyfried, N. E. Peters, B. T. Aulenbach, and R. Hooper (2011), Storage as a metric of catchment comparison, *Hydrol. Processes*, *25*(21), 3364-3371, doi:10.1002/hyp.8113.

Monteith, J. L. (1964), Evaporation and environment. The state and movement of water in living organisms, *Symp. Soc. Exp. Biol.*, *19*, 205.

Moore, R. (1985), The probability-distributed principle and runoff production at point and basin scales, *Hydrol. Sci. J.*, *30*, 273-297.

Moriasi, D. N., J. G. Arnold, M. W. Van Liew, R. L Bingner, R. D. Harmel, and T. L. Veith (2007), Model evaluation guidelines for systematic quantification of accuracy in watershed simulations, *Trans. ASABE*, *50*(3), 885-900.

Milly, P. C. D. (1994), Climate, soil water storage, and the average annual water balance, *Water Resour. Res.*, *30*(7), 2143-2156, doi:10.1029/94WR00586.

Milly, P. C. D., and Dunne, K. A. (2002), Macroscale water fluxes 2. Water and energy supply control of their interannual variability. *Water Resour. Res.*, *38*(10), 1206, doi:10.1029/2001WR000760

Nash, J.E. and J.V. Sutcliffe (1970), River flow forecasting through conceptual models part I-A discussion of principles, *J. Hydrol.*, *10*(3): 282-290.

Pardé, M. (1933), *Fleuves et Rivières*, vol. 1, Armand Colin, Paris.

Perdigão, R. A. P., and G. Blöschl (2014), Spatiotemporal flood sensitivity to annual precipitation: Evidence for landscape-climate coevolution, *Water Resour. Res.*, *50*, 54925509, doi:10.1002/2014WR015365.

Perrin, C., C. Michel, and V. Andreassian (2001), Does a large number of parameters enhance model performance? Comparative assessment of common catchment model structures on 429 catchments, *J. Hydrol.*, *242*, 275-301, doi:10.1016/S0022-1694(00)00393-0.

Petersen, T., N. Devineni, and A. Sankarasubramanian (2012), Seasonality of monthly runoff over the continental United States: Causality and relations to mean annual and mean monthly distributions of moisture and energy, *J. Hydrol.*, *468-469*, 139-150, https://doi.org/10.1016/j.jhydrol.2012.08.028

Porporato, A., E. Daly, and I. Rodriguez-Ignacio (2004), Soil water balance and ecosystem response to climate change, *Am. Nat.*, *164*(5), 625-632, doi:10.1086/424970.

Potter, N. J., L. Zhang, P. C. D. Milly, T. A. McMahon, and A. J. Jakeman (2005), Effects of rainfall seasonality and soil moisture capacity on mean annual water balance for Australian catchments, *Water Resour. Res.*, *41*, W06007,doi:10.1029/2004WR003697.

Potter, N. J., and L. Zhang(2009), Interannual variability of catchment water balance in Australia, *J. Hydrol.*, *369*(1-2), 120-129.

Razavi, S., and H. V. Gupta (2016), A new framework for comprehensive, robust, and efficient global sensitivity analysis: 2. Application, *Water Resour. Res.*, *52*, doi:10.1002/2015WR017559.

Reggiani, P., M. Sivapalan, and S. M. Hassanizadeh (2000), Conservation equations governing hillslope responses: Exploring the physical basis of water balance, *Water Resour. Res.*, *36*(7), 1845-1863, doi:10.1029/2000WR900066.

Rodriguez-Iturbe, I., A. Porporato, L. Ridolfi, V. Isham, and D. R. Cox (1999), Probabilistic modelling of water balance at a point: The role of climate, soil and vegetation, *Proc. R. Soc. London*, *Ser. A*, *455*, 3789-3805.

Rossi, M. W., K. X. Whipple, and E. R. Vivoni (2015), Precipitation and evapotranspiration controls on daily runoff variability in the contiguous United States and Puerto Rico, *J. Geophys. Res. Earth Surface, 121*, 128-145, doi:10.1002/2015JF003446.

SCS. (1972), *Hydrology. National Engineering Handbook, Supplement A, Section 4, Chapter 10.* Soil Conservation Service, US Department of Agriculture, Washington, DC.

Schaake, J. C., V. I. Koren, Q. Y. Duan, K. Mitchell, and F. Chen (1996), Simple water balance model for estimating runoff at different spatial and temporal scales, *J. Geophys. Res.*, 101, 7461-7475, doi:10.1029/95JD02892.

Shao, Q., A. Traylen, and L. Zhang (2012), Nonparametric method for estimating the effects of climatic and catchment characteristics on mean annual evapotranspiration, *Water Resour. Res.*, *48*, W03517, doi:10.1029/2010WR009610.

Sivapalan, M., G. Blöschl, R. Merz, and D. Gutknecht (2005), Linking flood frequency to long-term water balance: Incorporating effects of seasonality, *Water Resour. Res.*, *41*, W06012, doi:10.1029/2004WR003439.

Soylu, M. E., E. Istanbulluoglu, J. D. Lenters, and T. Wang (2011), Quantifying the impact of groundwater depth on evapotranspiration in a semi-arid grassland region, *Hydrol. Earth Syst. Sci.*, *15*(3), 787-806, doi:10.5194/hess-15-787-2011.

Sudheer, K. P., I. Chaubey, V. Garg, and K. W. Migliaccio (2007), Impact of timescale of the calibration objective function on the performance of watershed models, *Hydrol. Processes*, *21*(25), 3409-3419.

Thomas, H. A. (1981), Improved methods for national water assessment, report, *contract WR 15249270*, U.S. Water Resour. Counc., Washington, D. C.

Troch, P. A., F. P. De Troch, and W. Brutsaert (1993), Effective water table depth to describe initial conditions prior to storm rainfall in humid regions. *Water Resour. Res.*, *29*(2), 427-434.

Troch, P. A., G. Carrillo, M. Sivapalan, T. Wagner, and K. Sawicz (2013), Climate-vegetation-soil interactions and long-term hydrologic partitioning: Signatures of catchment co-evolution, *Hydrol. Earth Syst. Sci.*, *17*, 2209-2217.

Wang, D., and M. Hejazi (2011), Quantifying the relative contribution of the climate and direct human impacts on mean annual streamflow in the contiguous United States, *Water Resour. Res.*, *47*, W00J12, doi:10.1029/2010WR010283.

Wang, D., and Y. Tang (2014), A one-parameter Budyko model for water balance captures emergent behavior in Darwinian hydrologic models, *Geophys. Res. Lett.*, *41*(13), 4569-4577.

Wang, D. (2018), A new probability density function for spatial distribution of soil water storage capacity leads to the SCS curve number method, *Hydrol. Earth Syst. Sci.*, *22*, 6567-6578.

Wang, G., J. Xia, and J. Chen (2009), Quantification of effects of climate variations and human activities on runoff by a monthly water balance model: A case study of the Chaobai River basin in northern China, *Water Resour. Res.*,45, W00A11, doi :10.1029/2007WR006768.

Wang, Q., T. C. Pagano, S. Zhou, H. A. P. Hapuarachchi, L. Zhang, and D. E. Robertson (2011), Monthly versus daily water balance models in simulating monthly runoff, *J. Hydrol.*, *404*, 166-175, doi:10.1016/j.jhydrol.2011.04.027.

Westhoff, M., E. Zehe, P. Archambeau, and B. Dewals (2016), Does the Budyko curve reflect a maximum power state of hydrological systems? A backward analysis, *Hydrol. Earth Syst. Sci.*, *20*, 479-486.

Woods, R. A. (2009), Analytical model of seasonal climate impacts on snow hydrology: Continuous snowpacks, *Adv. Water Resour.*, *32*(10), 1465-1481, doi:10.1016/j.advwatres.2009.06.011.

Xu, X., D. Yang, and M. Sivapalan (2012), Assessing the impact of climate variability on catchment water balance and vegetation cover, *Hydrol. Earth Syst. Sci.*, *16*(1), 43-58.

Yang, D., F. Sun, Z. Liu, Z. Cong, and Z. Lei (2006), Interpreting the complementary relationship in non-humid environments based on the Budyko and Penman hypotheses, *Geophys. Res. Lett.*, *33*, L18402, doi:10.1029/2006GL027657.

Yang, D., F. Sun, Z. Liu, Z. Cong, G. Ni, and Z. Lei (2007), Analyzing spatial and temporal variability of annual water-energy balance in nonhumid regions of China using the Budyko hypothesis, *Water Resour. Res.*, *43*, W04426, doi:10.1029/2006WR005224.

Yang, H., D. Yang, Z. Lei, and F. Sun (2008), New analytical derivation of the mean annual water-energy balance equation, *Water Resour. Res.*, *44*, W03410, doi:10.1029/2007WR006135.

Yaeger, M., E. Coopersmith, S. Ye, L. Cheng, A. Viglione, and M. Sivapalan (2012), Exploring the physical controls of regional patterns of flow duration curves–Part 4: A synthesis of empirical analysis, process modeling and catchment classification, *Hydrol. Earth Syst. Sci.*, *16*(11), 4483-4498.

Yokoo, Y., M. Sivapalan, and T. Oki (2008), Investigating the roles of climate seasonality and landscape characteristics on mean annual and monthly water balances, *J. Hydrol.*, *357*(3-4), 255-269.

Zanardo, S., C. J. Harman, P. A. Troch, P. S. C. Rao, and M. Sivapalan (2012), Intra-annual rainfall variability control on interannual variability of catchment water balance: A stochastic analysis, *Water Resour. Res.*, *48*, W00J16, doi:10.1029/2010WR009869.

Zhang, L., W. R. Dawes, and G. R. Walker (2001), Response of mean annual evapotranspiration to vegetation changes at catchment scale, *Water Resour. Res.*, *37*(3), 701-708.

Zhang, L., N., Potter, K. Hickel, Y. Q. Zhang and Q. X. Shao (2008), Water balance modeling over variable time scales based on the Budyko framework-Model development and testing, *J. Hydrol.*, *360*(1-4), 117-131.

Figure captions:

Figure 1: The structure of the daily water balance model which unifies the probability distributed model (PDM) and SCS curve number method. C is soil water storage capacity at a point; $F(C)$ is the fraction of the catchment area for which the storage capacity is less than or equal to C; S_0 is the initial soil water storage; P is the precipitation which is partitioned into is the soil wetting (W) and runoff (R); E is the actual evaporation; γ is the partitioning parameter of runoff between the direct runoff (R_d) and groundwater recharge (R_g); S_d and S_g are the storages in the quick storage tank and slow storage tank, respectively; k_d and k_b are the runoff coefficients of direct runoff and base flow, respectively; Q_d, Q_b, and Q are the flow rates of direct runoff, base flow, and total runoff at the catchment outlet, respectively.

Figure 2: Evaporation is calculated based on the cumulative distribution function of soil water capacity when (a) the entire catchment is saturated and (b) the catchment is partially saturated. S_b is the average soil water storage capacity over the catchment; E_p is the potential evapotranspiration; E_s is the average evaporation over the catchment when the entire catchment is saturated.

Figure 3: Examples of different temporal patterns of climate inputs for Caney River in Kansas (USGS gage number: 07172000) during the period of 2000-2002: (a) daily climate; (b) monthly climate; (c) inter-annual climate; and (d) mean climate. The blue solid line represents precipitation (P) and the red dashed line represents potential evapotranspiration (E_p).

Figure 4: The flow charts for quantifying: (a) the relative effects of different climate variabilities on the daily runoff; (b) the relative effects of different components on the mean annual runoff. ρ denotes the effects of climate variability or other catchment characteristics considered in this study; Q_D, Q_M, Q_I, Q_S, Q_L are the 5 components of the total mean annual runoff that caused by the daily climate variability, monthly climate variability, inter-annual climate variability, storage capacity with its spatial variability, and long-term mean climate, respectively.

Figure 5: The performance of the water balances at different timescales: (a) *NSE* of the runoffs during the calibration period, (b) *NSE* of the runoffs during the validation period, (c) a comparison of the observed and calculated mean annual runoff during the validation period, and (d) the cumulative distribution of model bias during the validation period.

Figure 6: The relative roles of climate variability on runoff variabilities at the (a) daily, (b) monthly, (c) annual, and (d) mean annual scales.

Figure 7: Controls of different timescale climate variabilities on (a) daily runoff during 2010-2012; (b) mean Pardé coefficient for each month during the 2000-2015; and (c) annual runoff during 2000-2015 in Smith River, California (USGS gage number: 11532500).

Figure 8: (a) The relationship between the relative role of monthly climate variability on monthly runoff and climate aridity index (E_p/P); (b) the relationship between the relative role of inter-annual climate variability on annual runoff and E_p/P; (c) the relationship between the relative role of monthly climate variability on annual runoff and E_p/P; and (d) the relationship between

the sensitivity of annual runoff to climate variabilities and the E_p/P with base flow index indicated by the colors of the dots, and with two insets showing (d-1) the relationship between the Hurst exponent of runoff and the base flow index, and (d-2) the relationship between the Hurst exponents of runoff and that of precipitation.

Figure 9: The relative roles of daily, monthly, inter-annual climate variability, mean climate, soil water storage capacity and its spatial variability on the mean annual runoff across the catchments.

Figure 10: The effects of soil water storage capacity and its spatial variability, mean climate, inter-annual climate variability, monthly climate variability, and daily climate variability on the mean annual evaporation ratio (E/P) in the Budyko framework.

Figure 11: The relationships between the climate aridity index (E_p/P) and the relative roles of (a) mean climate, (b) soil water storage capacity and its spatial variability, (c) inter-annual climate variability, (d) monthly climate variability, and (e) daily climate variability on the mean annual runoff.

Figure 12: Climate inputs at different timescales (left column) and their corresponding water balance model structures (right column): (a) daily model; (b) monthly model; (c) annual model; (d) mean annual model.

Table 1: The ranges and units of parameters for the daily water balance model [*Kollat et al.*, 2012; *Wang*, 2018], and the calibrated parameter values for 12 selected catchments (locations shown in Figure 10).

Index	**USGS gage number**	**Parameter and range**				
		S_b [mm]	a [-]	γ [-]	k_b [day^{-1}]	k_d [day^{-1}]
		[50-1500]	(0-2)	[0-1]	[0-0.14)	[0.14-1]
(1)	11532500	1366.7	1.9979	0.8689	0.0002	0.2509
(2)	12027500	775.2	1.9841	0.9989	0.1388	0.1741
(3)	03512000	581.3	1.9396	0.6140	0.0306	0.2703
(4)	03161000	531.5	1.9726	0.5727	0.0069	0.2788
(5)	03574500	370.7	1.9866	0.9990	0.1324	0.2540
(6)	03109500	410.3	1.9631	0.9990	0.1133	0.2042
(7)	03269500	335.9	1.9464	0.5782	0.0052	0.2554
(8)	05520500	295.1	1.9439	0.3364	0.0122	0.1402
(9)	07186000	441.0	1.9858	0.9988	0.1376	0.2928
(10)	06894000	293.9	1.9403	0.9999	0.0829	0.3735
(11)	08033500	878.7	1.9888	0.0014	0.0810	0.1628
(12)	07172000	235.6	1.9419	0.9989	0.1345	0.3622

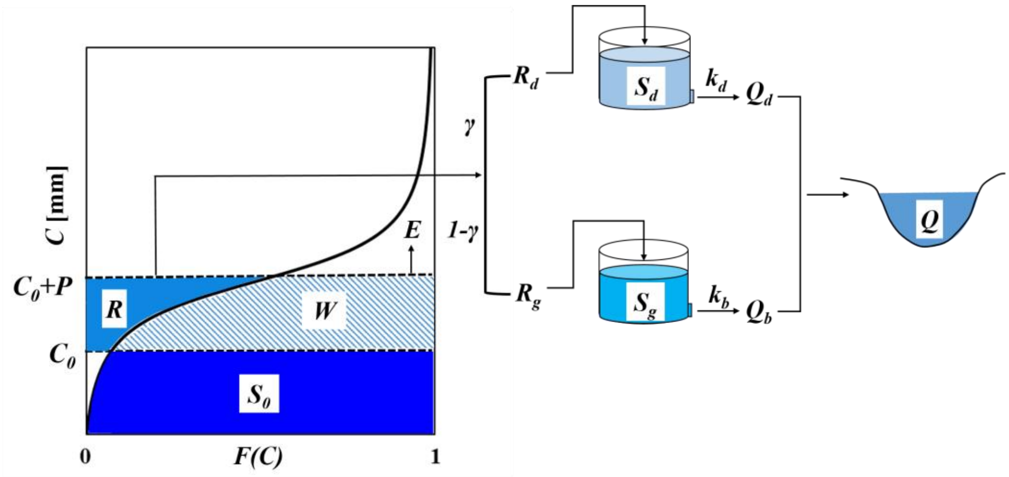

Figure 1: The structure of the daily water balance model which unifies the probability distributed model (PDM) and SCS curve number method. C is soil water storage capacity at a point; $F(C)$ is the fraction of the catchment area for which the storage capacity is less than or equal to C; S_0 is the initial soil water storage; P is the precipitation which is partitioned into is the soil wetting (W) and runoff (R); E is the actual evaporation; γ is the partitioning parameter of runoff between the direct runoff (R_d) and groundwater recharge (R_g); S_d and S_g are the storages in the quick storage tank and slow storage tank, respectively; k_d and k_b are the runoff coefficients of direct runoff and base flow, respectively; Q_d, Q_b, and Q are the flow rates of direct runoff, base flow, and total runoff at the catchment outlet, respectively.

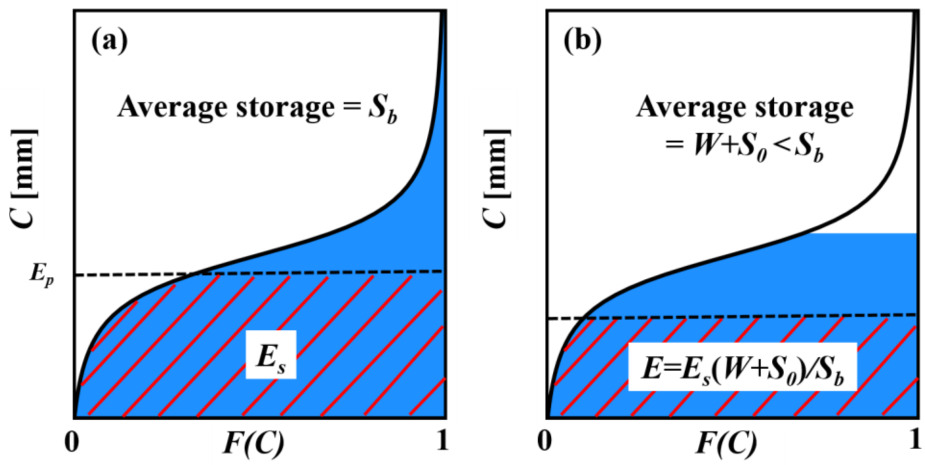

Figure 2: Evaporation is calculated based on the cumulative distribution function of soil water capacity when (a) the entire catchment is saturated and (b) the catchment is partially saturated. S_b is the average soil water storage capacity over the catchment; E_p is the potential evapotranspiration; E_s is the average evaporation over the catchment when the entire catchment is saturated.

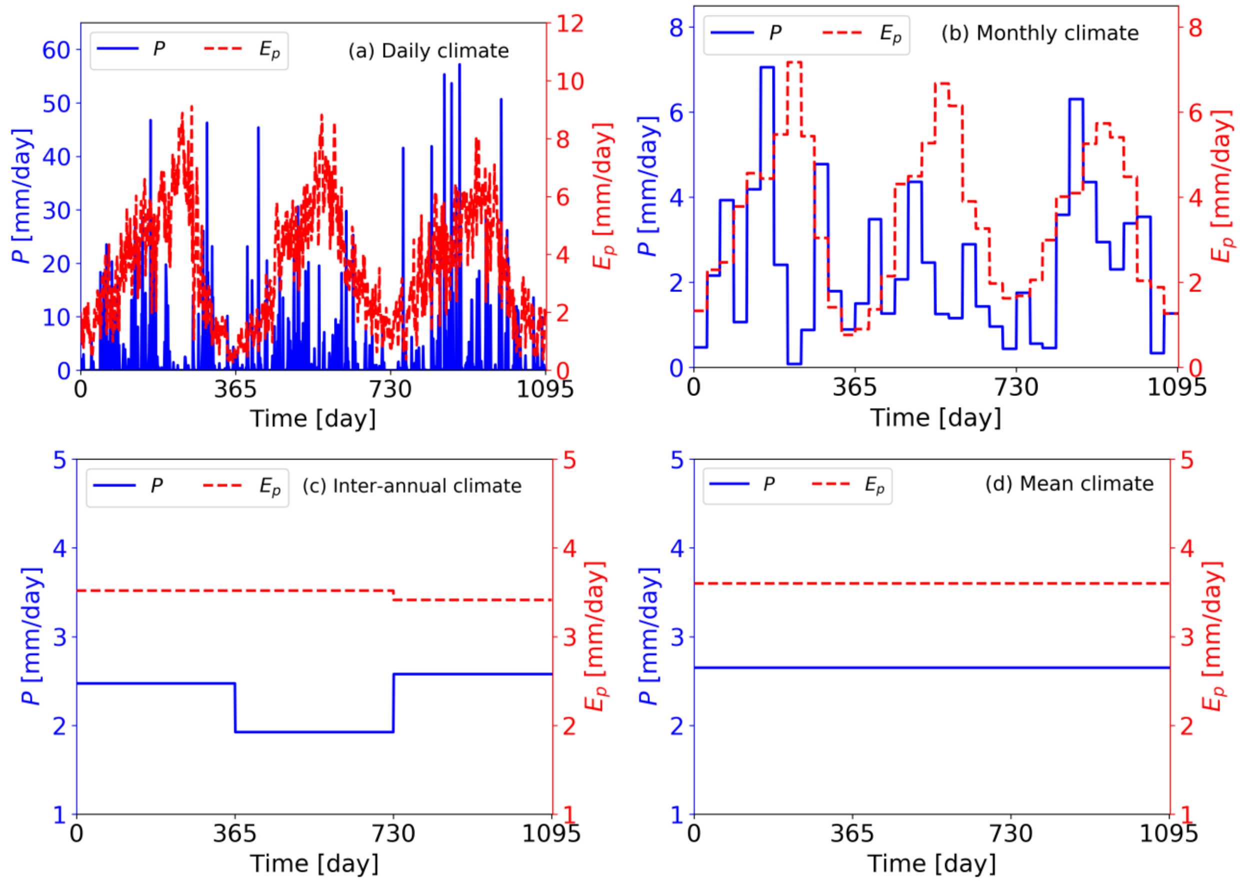

Figure 3: Examples of different temporal patterns of climate inputs for Caney River in Kansas (USGS gage number: 07172000) during the period of 2000-2002: (a) daily climate; (b) monthly climate; (c) inter-annual climate; and (d) mean climate. The blue solid line represents precipitation (P) and the red dashed line represents potential evapotranspiration (E_p).

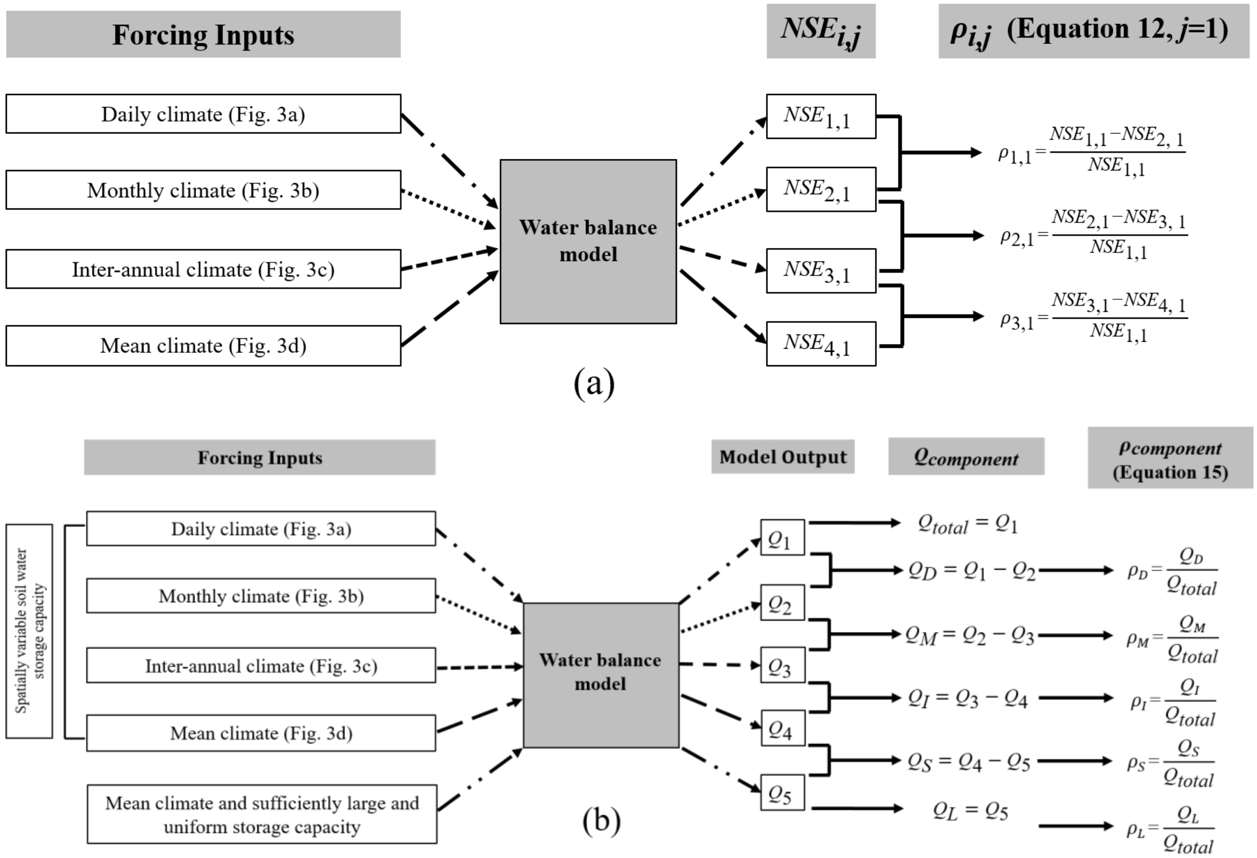

Figure 4: The flow charts for quantifying: (a) the relative effects of different climate variabilities on the daily runoff; (b) the relative effects of different components on the mean annual runoff. ρ denotes the effects of climate variability or other catchment characteristics considered in this study; Q_D, Q_M, Q_I, Q_S, Q_L are the 5 components of the total mean annual runoff that caused by the daily climate variability, monthly climate variability, inter-annual climate variability, storage capacity with its spatial variability, and long-term mean climate, respectively.

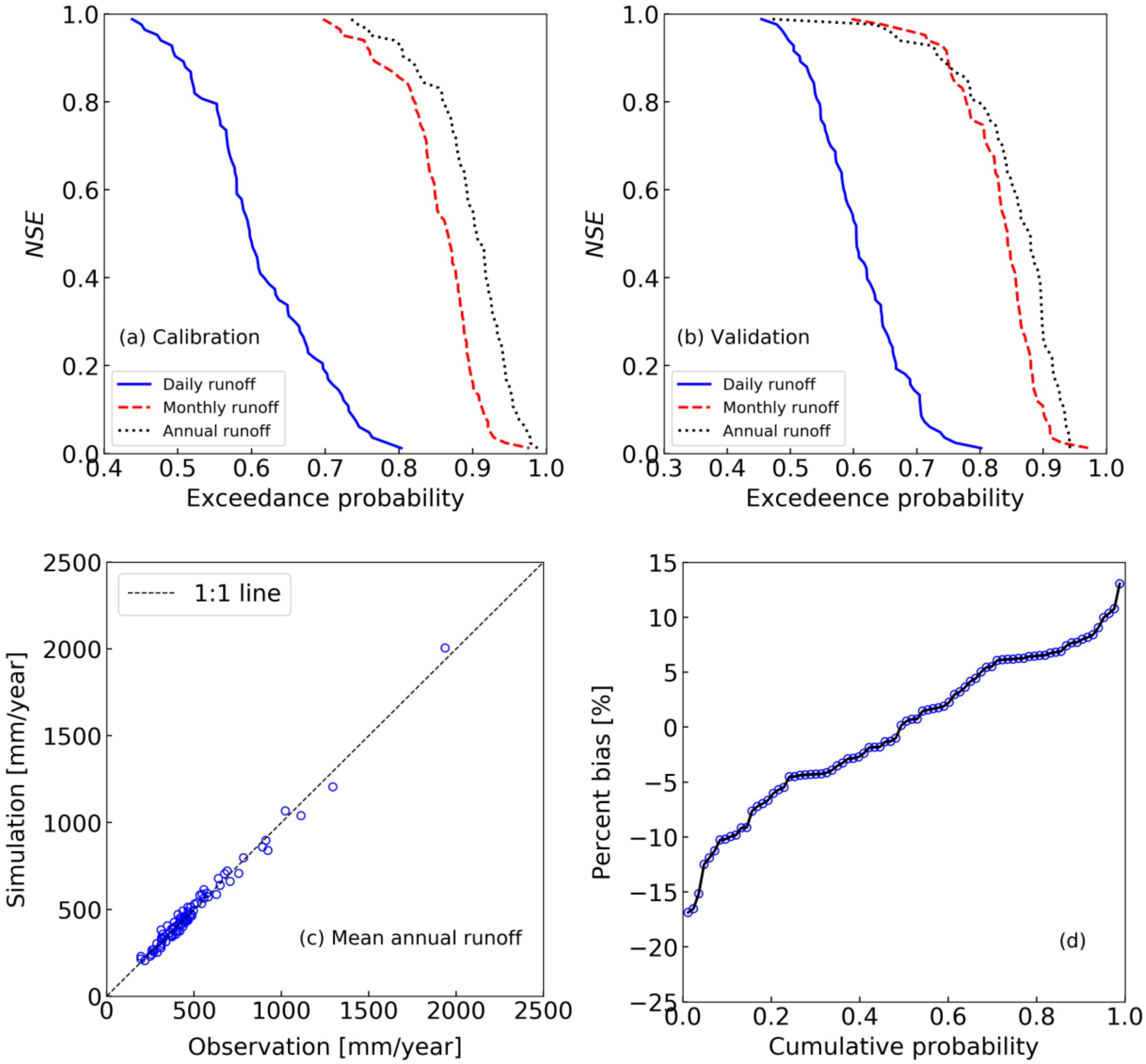

Figure 5: The performance of the water balances at different timescales: (a) *NSE* of the runoffs during the calibration period, (b) *NSE* of the runoffs during the validation period, (c) a comparison of the observed and calculated mean annual runoff during the validation period, and (d) the cumulative distribution of model bias during the validation period.

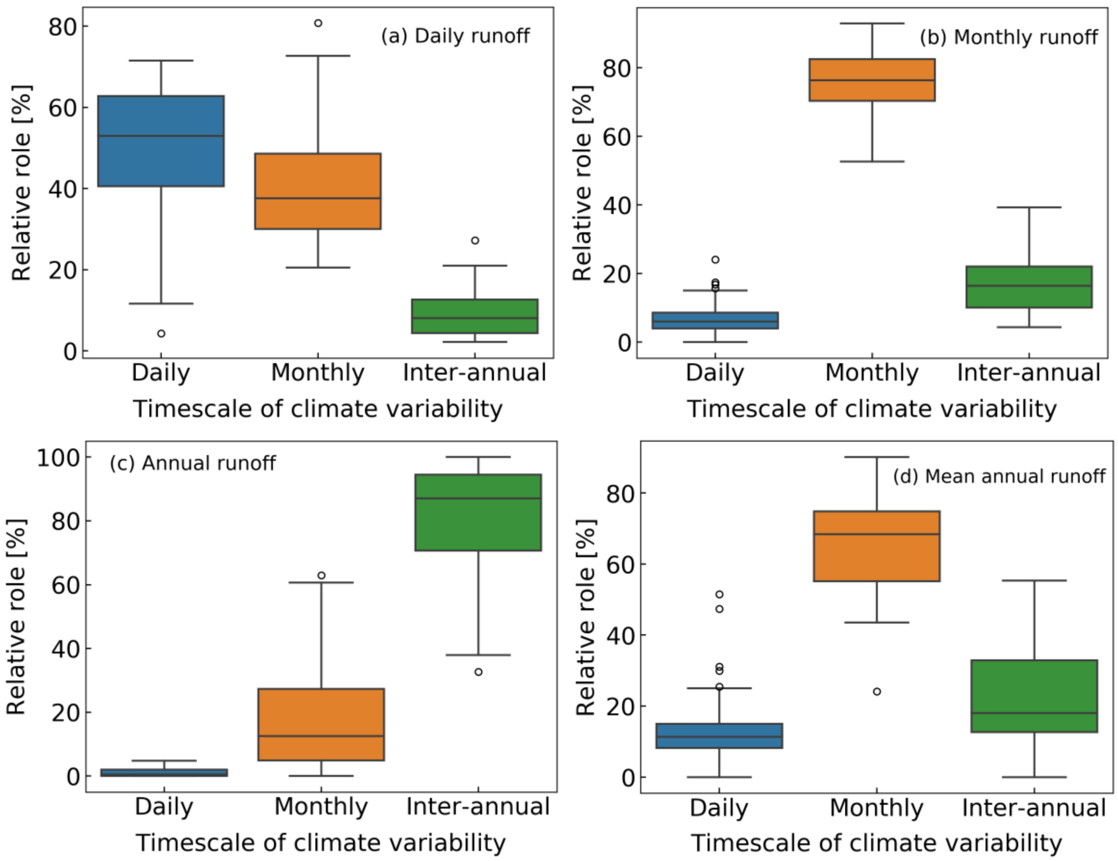

Figure 6: The relative roles of climate variability on runoff at the (a) daily, (b) monthly, (c) annual, and (d) mean annual scales.

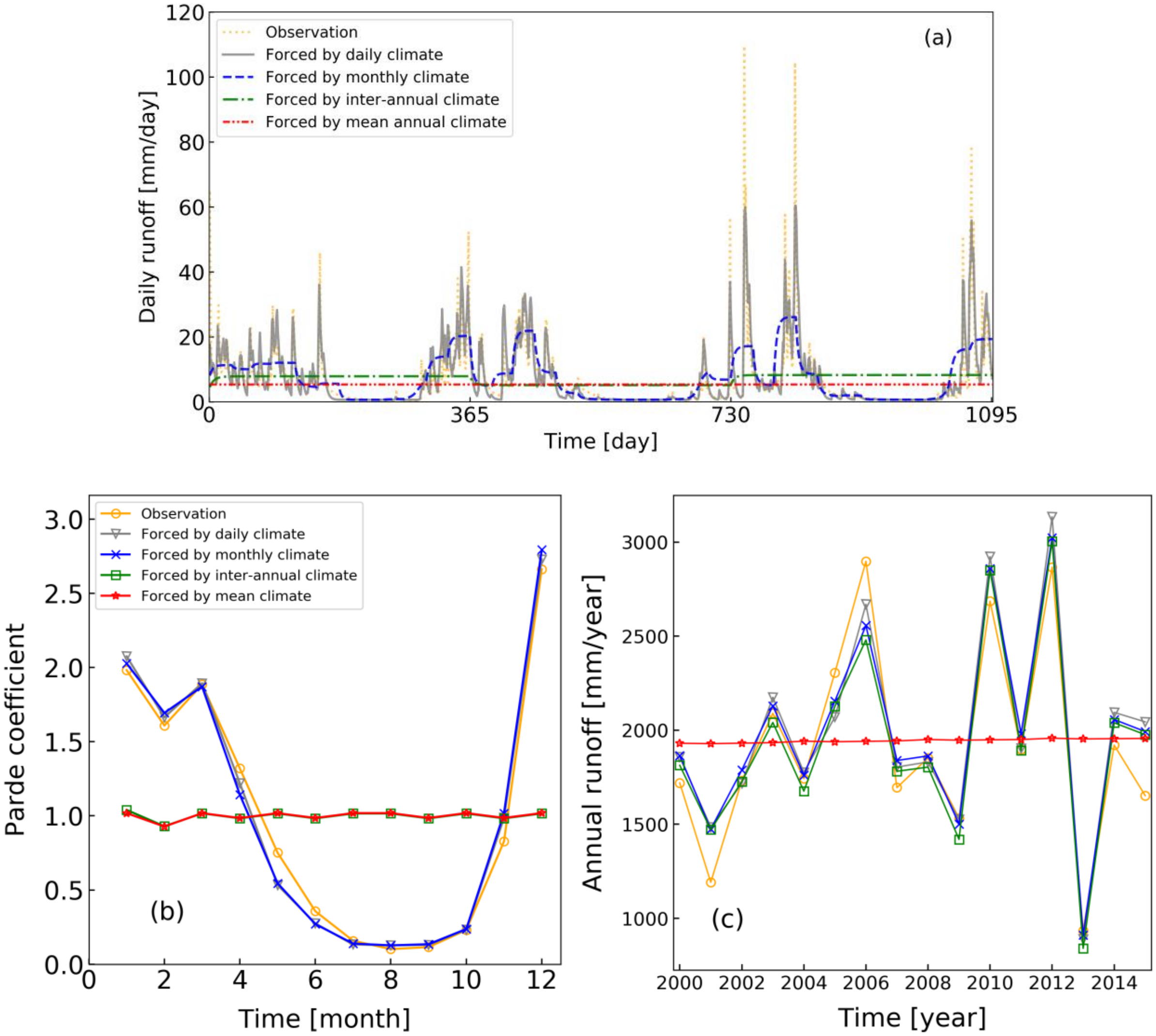

Figure 7: Controls of different timescale climate variabilities on (a) daily runoff during 2010-2012; (b) mean Pardé coefficient for each month during the 2000-2015; and (c) annual runoff during 2000-2015 in Smith River, California (USGS gage number: 11532500).

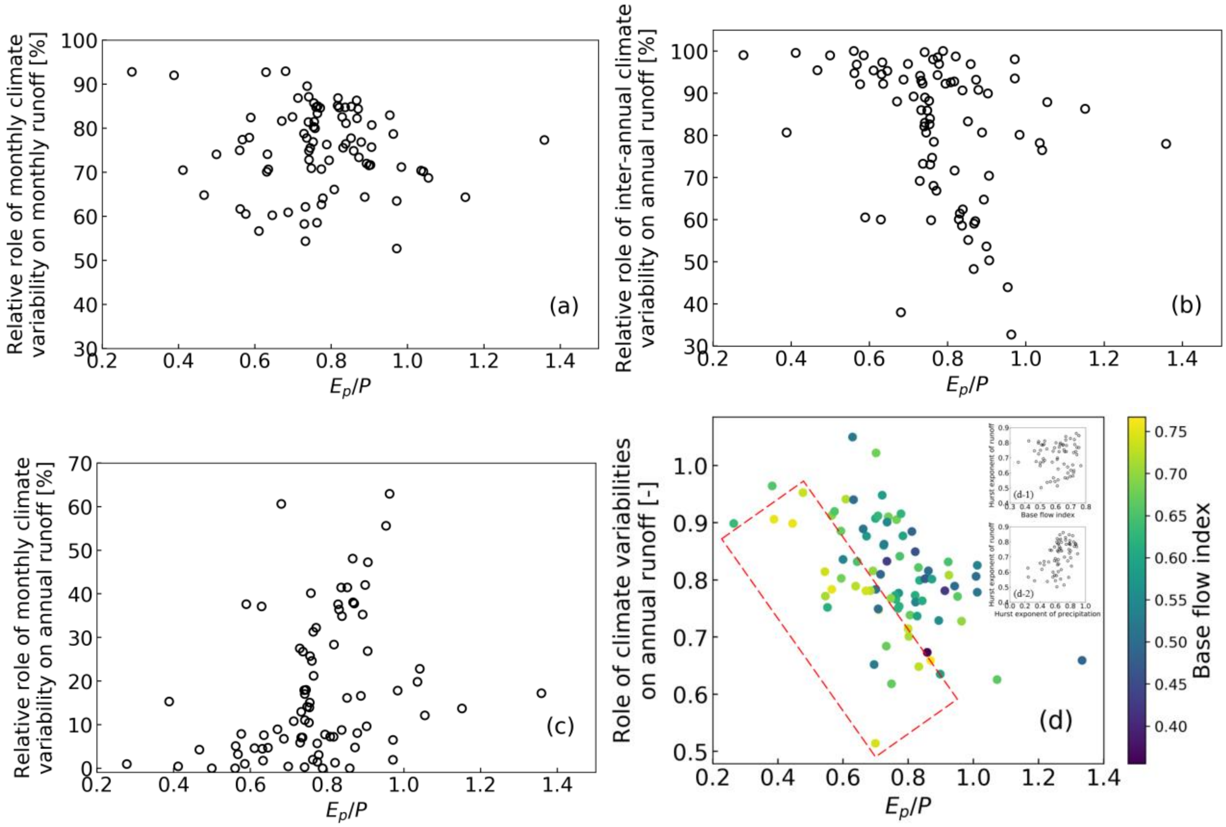

Figure 8: (a) The relationship between the relative role of monthly climate variability on monthly runoff and climate aridity index (E_p/P); (b) the relationship between the relative role of inter-annual climate variability on annual runoff and E_p/P; (c) the relationship between the relative role of monthly climate variability on annual runoff and E_p/P; and (d) the relationship between the sensitivity of annual runoff to climate variabilities and the E_p/P with base flow index indicated by the colors of the dots, and with two insets showing (d-1) the relationship between the Hurst exponent of runoff and the base flow index, and (d-2) the relationship between the Hurst exponents of runoff and that of precipitation.

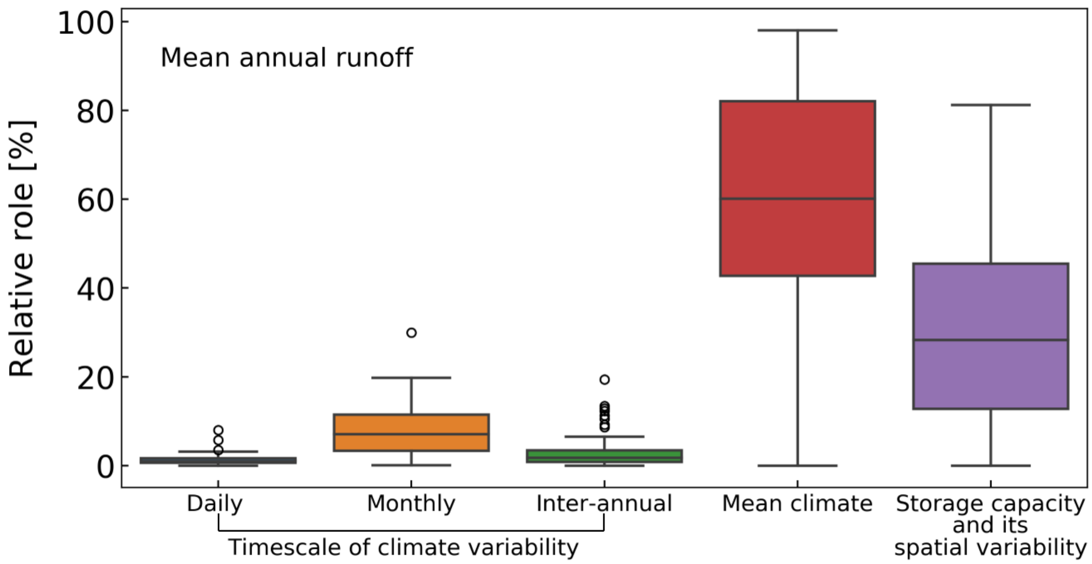

Figure 9: The relative roles of daily, monthly, inter-annual climate variability, mean climate, soil water storage capacity and its spatial variability on the mean annual runoff across the catchments.

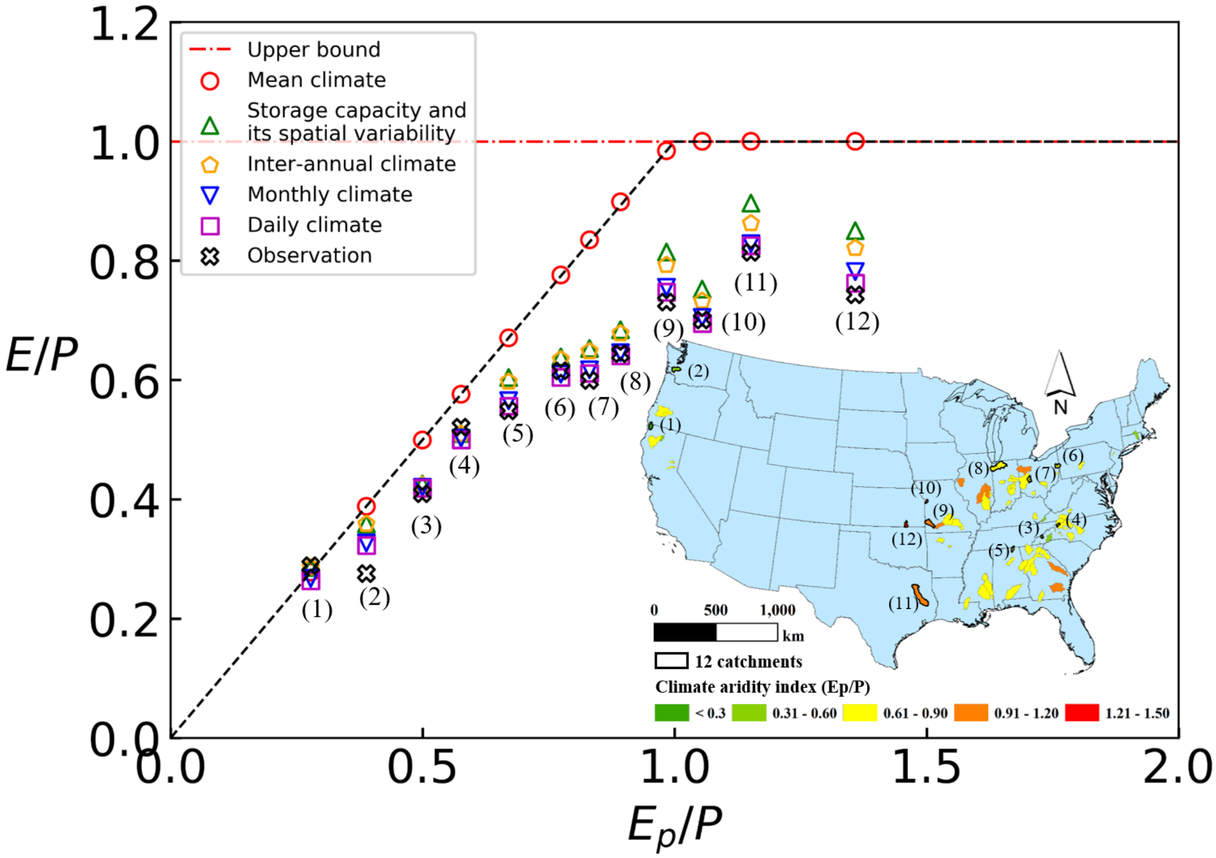

Figure 10: The effects of soil water storage capacity and its spatial variability, mean climate, inter-annual climate variability, monthly climate variability, and daily climate variability on the mean annual evaporation ratio (*E/P*) in the Budyko framework.

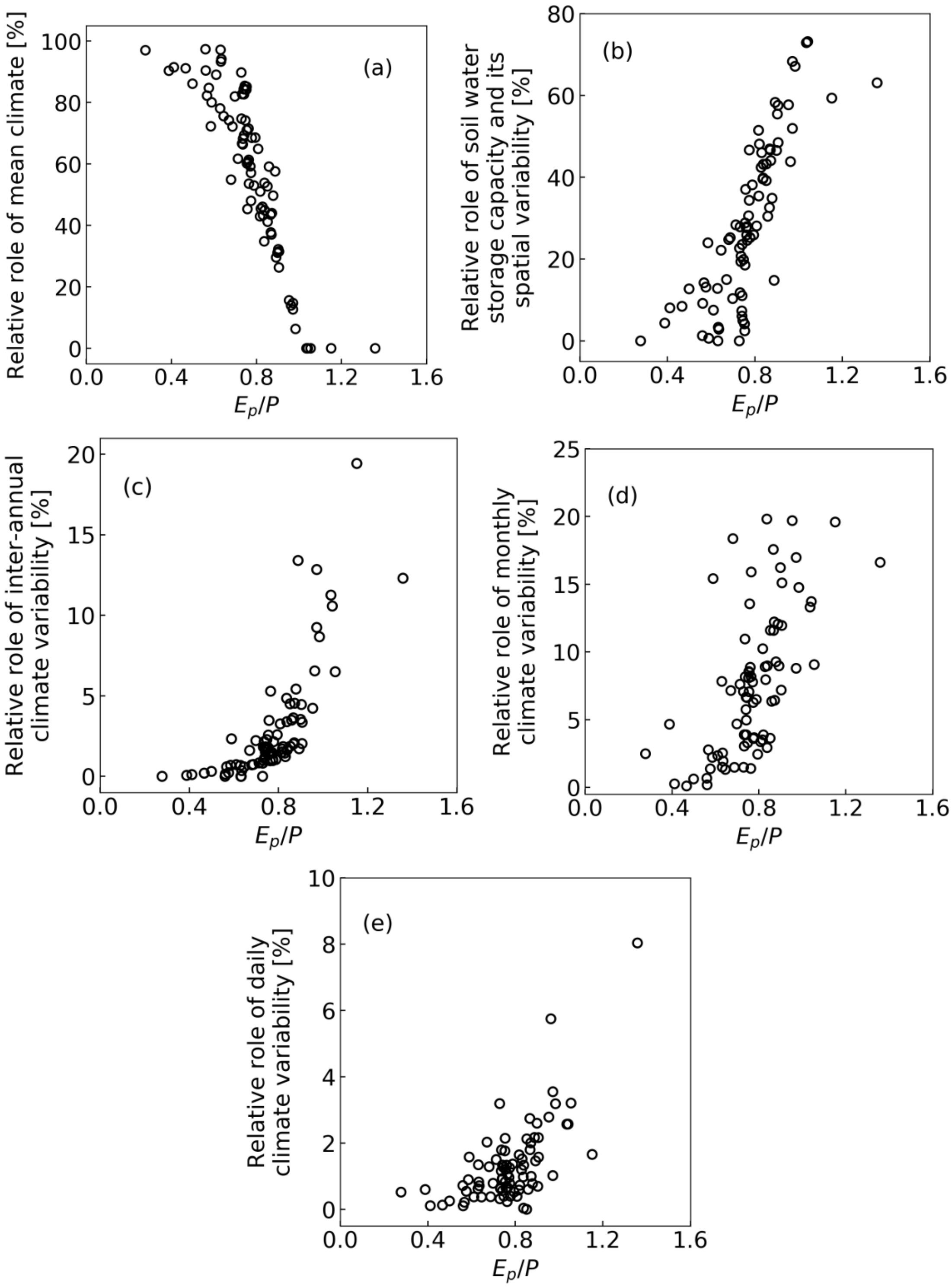

Figure 11: The relationships between the climate aridity index (E_p/P) and the relative effects of (a) mean climate, (b) soil water storage capacity and its spatial variability, (c) inter-annual climate variability, (d) monthly climate variability, and (e) daily climate variability on the mean annual runoff.

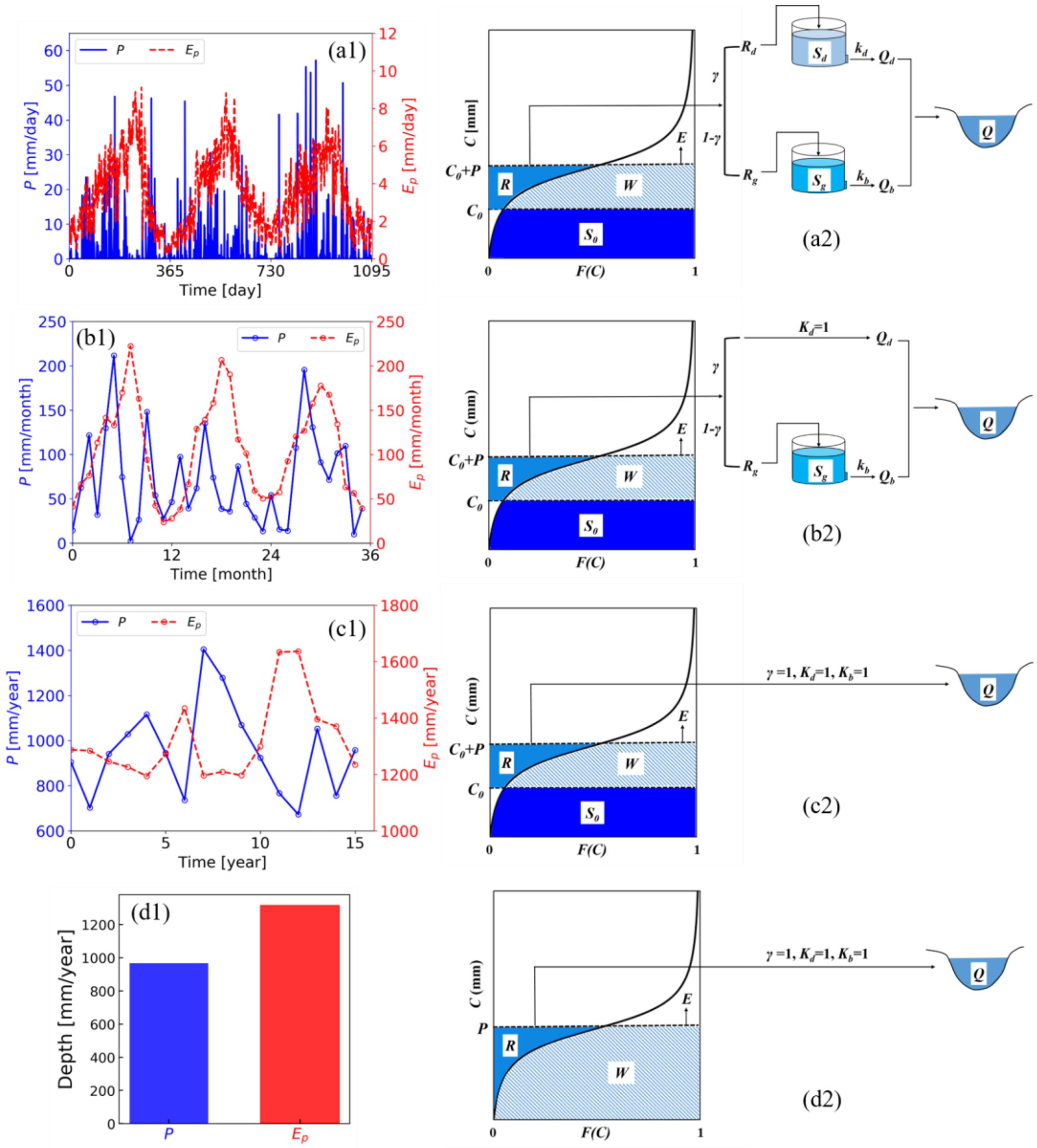

Figure 12: Climate inputs at different timescales (left column) and their corresponding water balance model structures (right column): (a) daily model; (b) monthly model; (c) annual model; (d) mean annual model.

Figure 1.

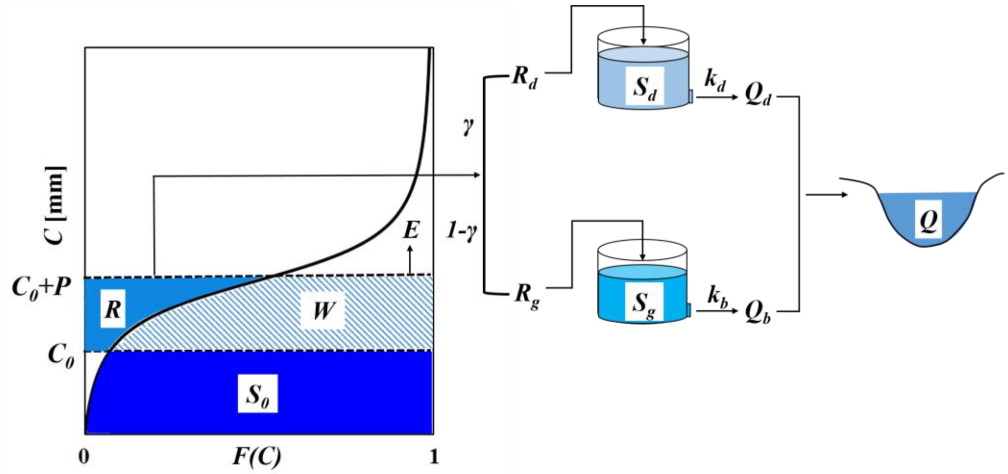

C [mm]
C0+P
C0
R
W
S0
E
0
F(C)
1
γ
1-γ
Rd
Rg
Sd
Sg
kd
kb
Qd
Qb
Q

Figure 2.

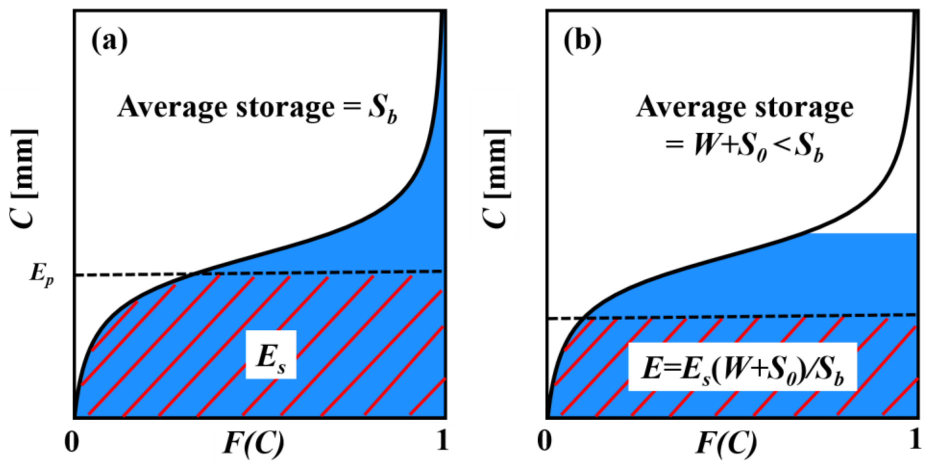

(a)
Average storage = S_b
C [mm]
E_p
E_s
0
$F(C)$
1
(b)
Average storage
= $W+S_0 < S_b$
C [mm]
$E=E_s(W+S_0)/S_b$
0
$F(C)$
1

Figure 3.

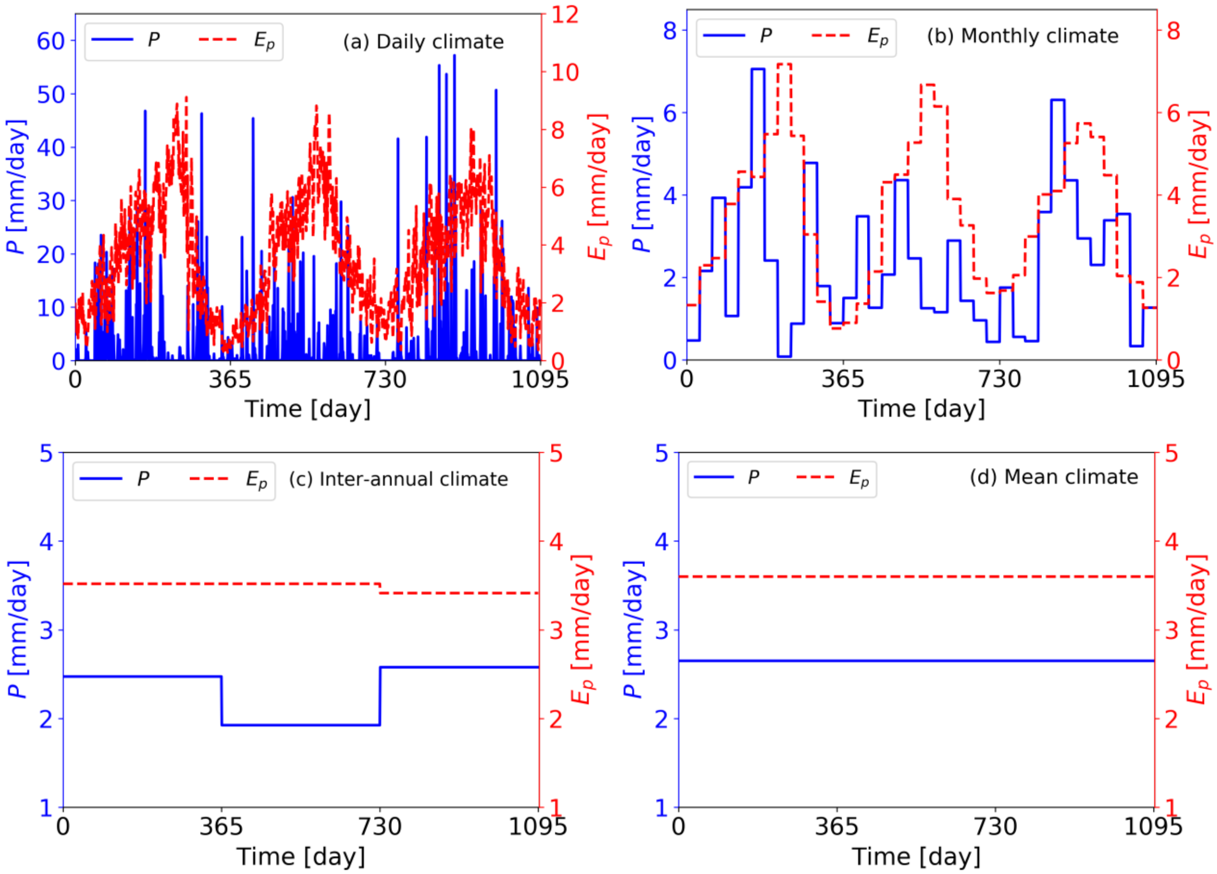

(a) Daily climate
(b) Monthly climate
(c) Inter-annual climate
(d) Mean climate
P
E_p
P [mm/day]
E_p [mm/day]
Time [day]
0
365
730
1095

Figure 4.

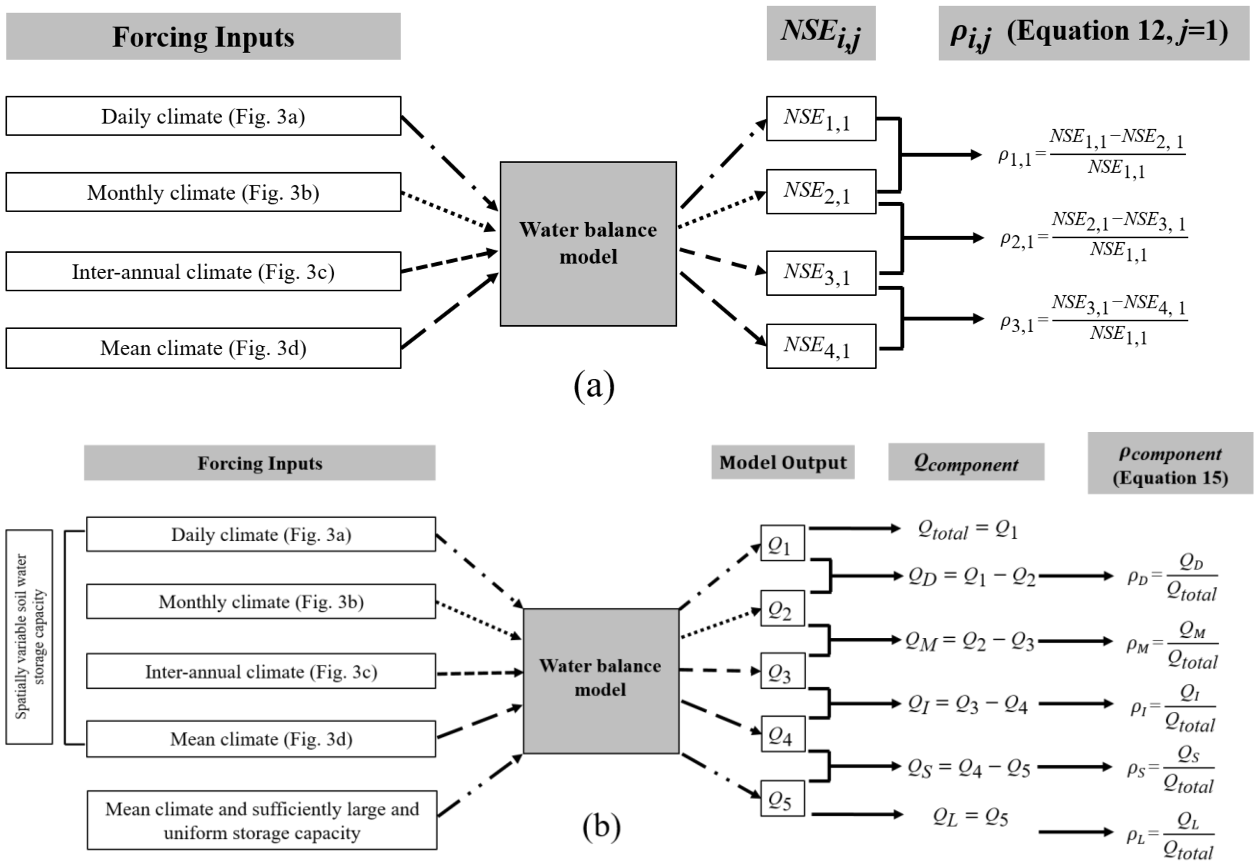
Forcing Inputs
NSEi,j
ρi,j (Equation 12, j=1)
Daily climate (Fig. 3a)
Monthly climate (Fig. 3b)
Inter-annual climate (Fig. 3c)
Mean climate (Fig. 3d)
Water balance model
NSE1,1
NSE2,1
NSE3,1
NSE4,1
ρ1,1 = (NSE1,1 − NSE2,1) / NSE1,1
ρ2,1 = (NSE2,1 − NSE3,1) / NSE1,1
ρ3,1 = (NSE3,1 − NSE4,1) / NSE1,1
(a)
Forcing Inputs
Model Output
Qcomponent
ρcomponent (Equation 15)
Spatially variable soil water storage capacity
Daily climate (Fig. 3a)
Monthly climate (Fig. 3b)
Inter-annual climate (Fig. 3c)
Mean climate (Fig. 3d)
Mean climate and sufficiently large and uniform storage capacity
Water balance model
Q1
Q2
Q3
Q4
Q5
Qtotal = Q1
QD = Q1 − Q2
QM = Q2 − Q3
QI = Q3 − Q4
QS = Q4 − Q5
QL = Q5
ρD = QD / Qtotal
ρM = QM / Qtotal
ρI = QI / Qtotal
ρS = QS / Qtotal
ρL = QL / Qtotal
(b)

Figure 5.

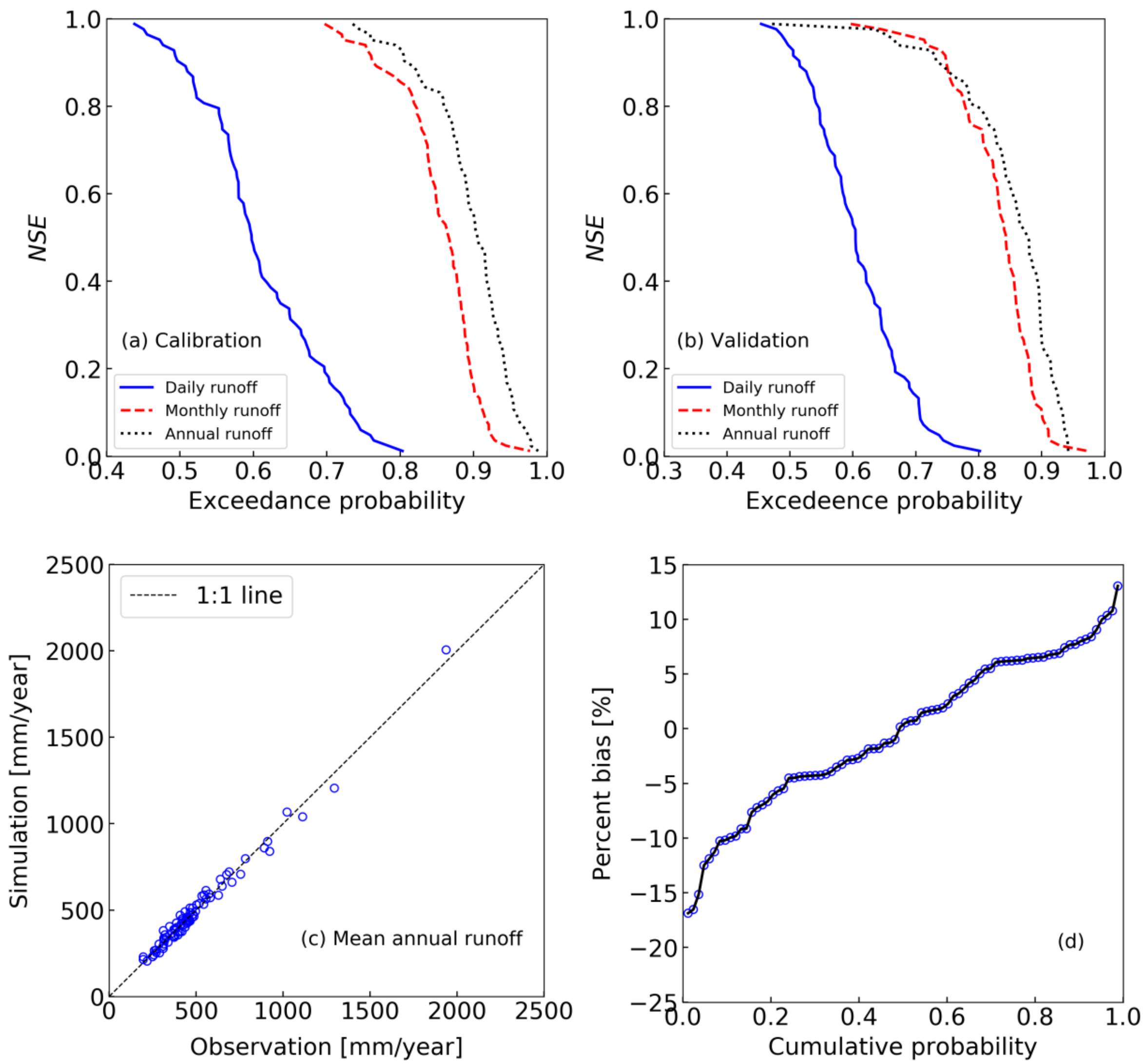
NSE
Exceedance probability
(a) Calibration
Daily runoff
Monthly runoff
Annual runoff
Excedeence probability
(b) Validation
Simulation [mm/year]
Observation [mm/year]
1:1 line
(c) Mean annual runoff
Percent bias [%]
Cumulative probability
(d)

Figure 6.

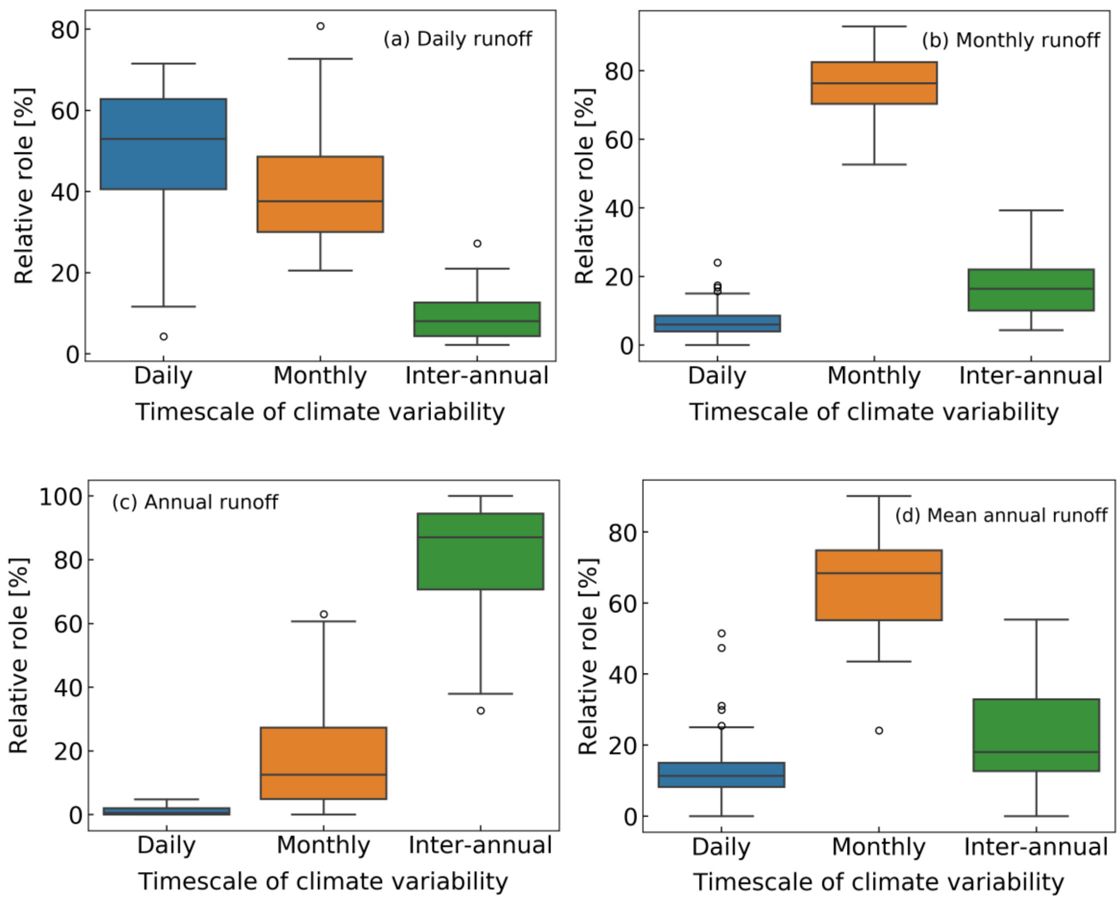

(a) Daily runoff
(b) Monthly runoff
(c) Annual runoff
(d) Mean annual runoff
Relative role [%]
Daily
Monthly
Inter-annual
Timescale of climate variability

Figure 7.

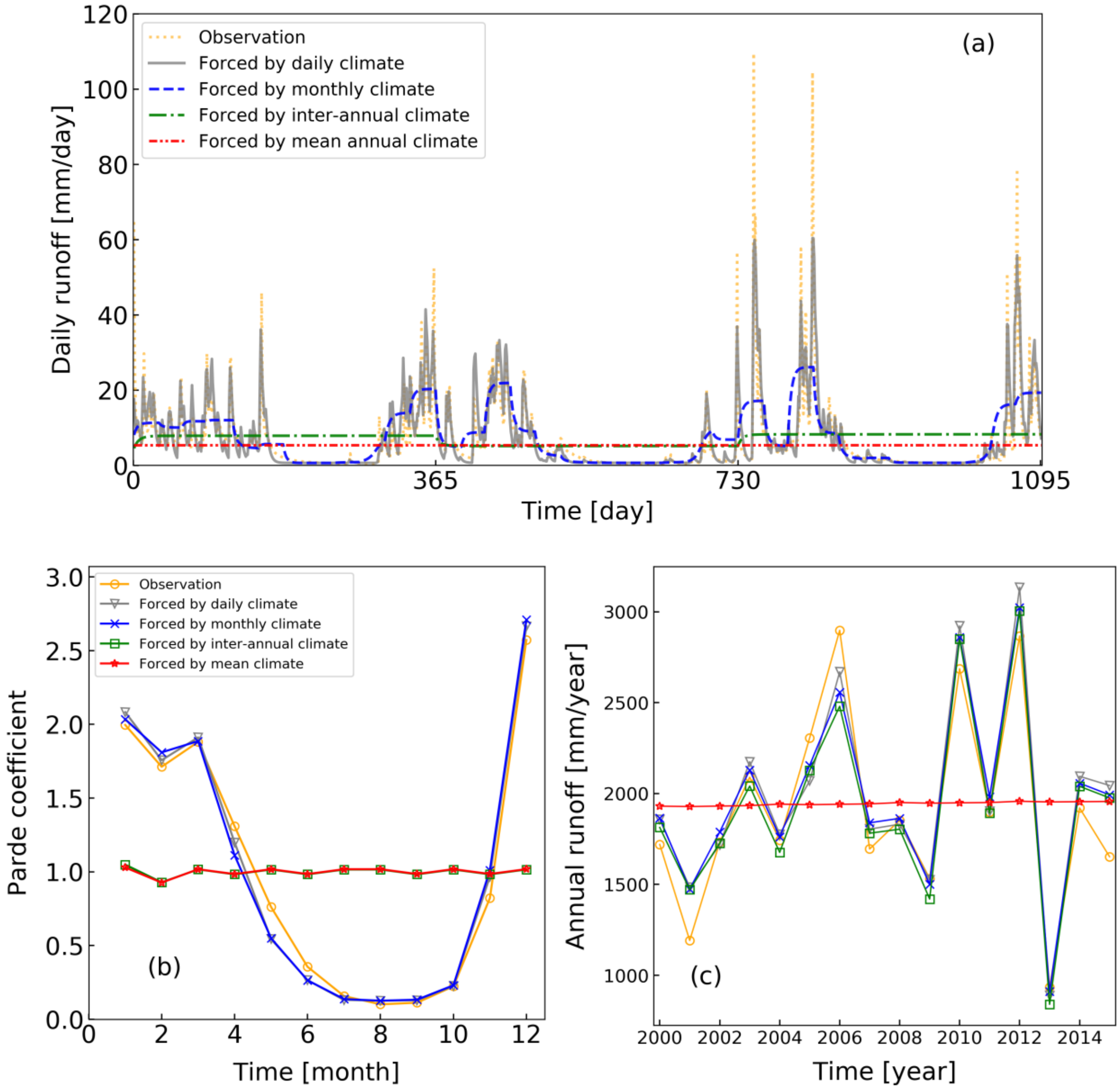

Daily runoff [mm/day]
Time [day]
(a)
Observation
Forced by daily climate
Forced by monthly climate
Forced by inter-annual climate
Forced by mean annual climate
0
20
40
60
80
100
120
0
365
730
1095
Parde coefficient
Time [month]
(b)
Observation
Forced by daily climate
Forced by monthly climate
Forced by inter-annual climate
Forced by mean climate
0.0
0.5
1.0
1.5
2.0
2.5
3.0
0
2
4
6
8
10
12
Annual runoff [mm/year]
Time [year]
(c)
1000
1500
2000
2500
3000
2000
2002
2004
2006
2008
2010
2012
2014

Figure 8.

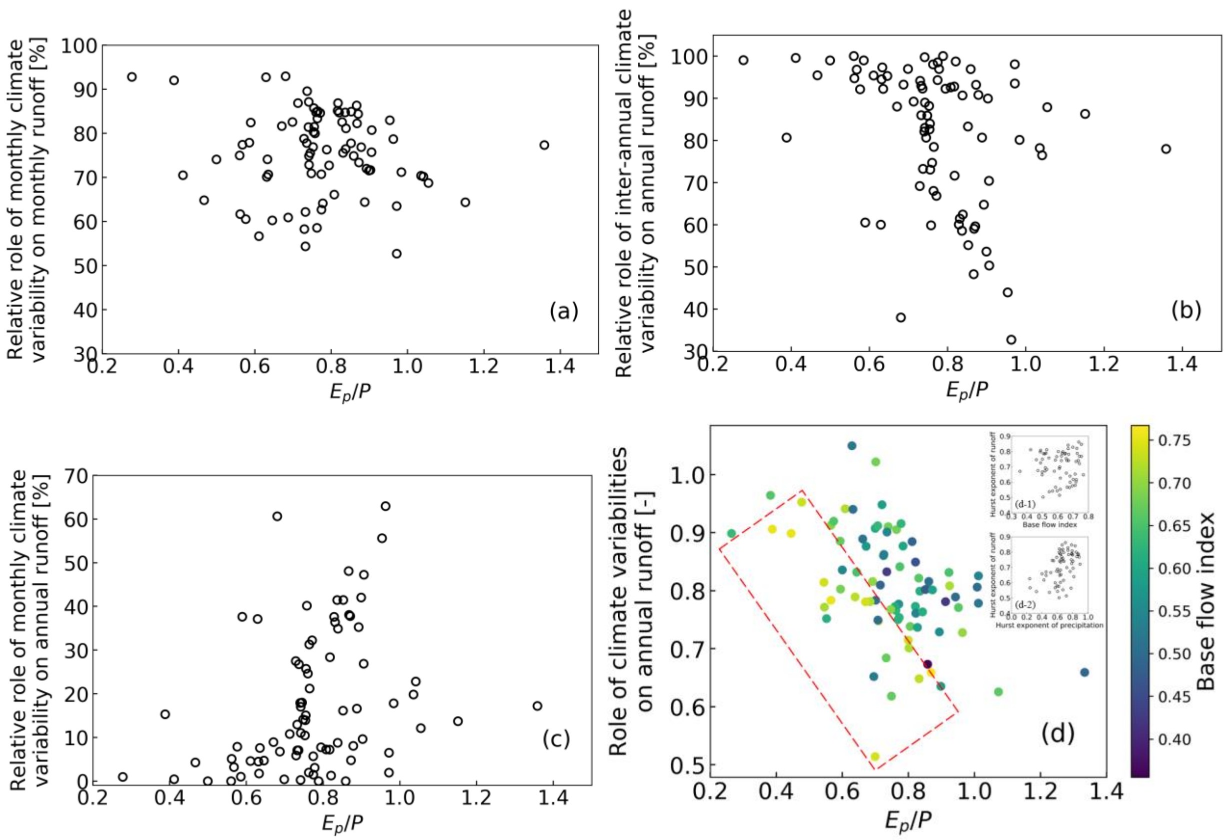

Relative role of monthly climate variability on monthly runoff [%]
(a)
Relative role of inter-annual climate variability on annual runoff [%]
(b)
Relative role of monthly climate variability on annual runoff [%]
(c)
Role of climate variabilities on annual runoff [-]
(d)
(d-1)
(d-2)
Base flow index
Hurst exponent of runoff
Hurst exponent of precipitation
E_p/P

Figure 9.

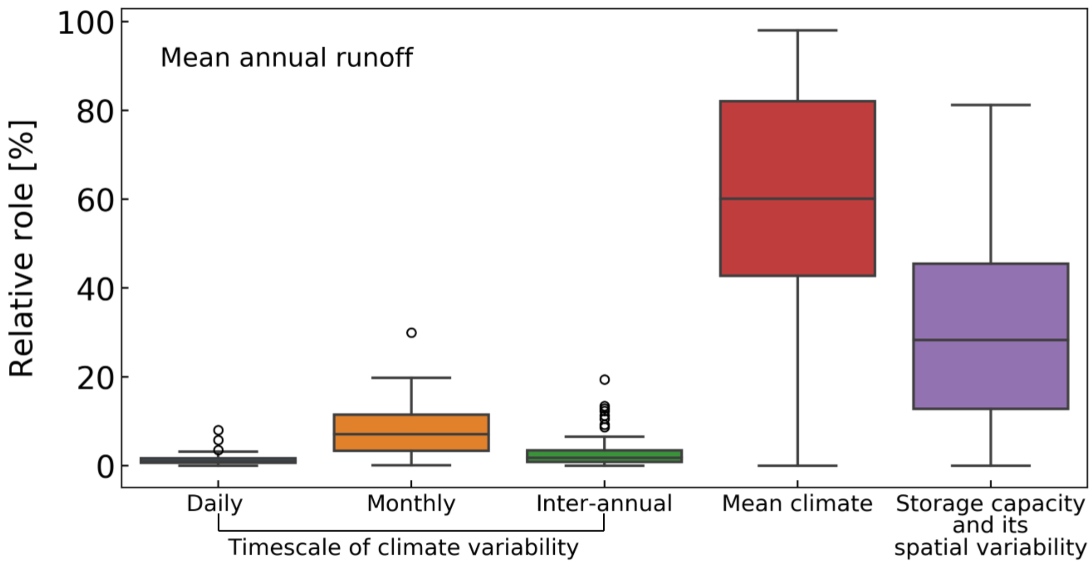

Mean annual runoff
Relative role [%]
100
80
60
40
20
0
Daily
Monthly
Inter-annual
Mean climate
Storage capacity and its spatial variability
Timescale of climate variability

Figure 10.

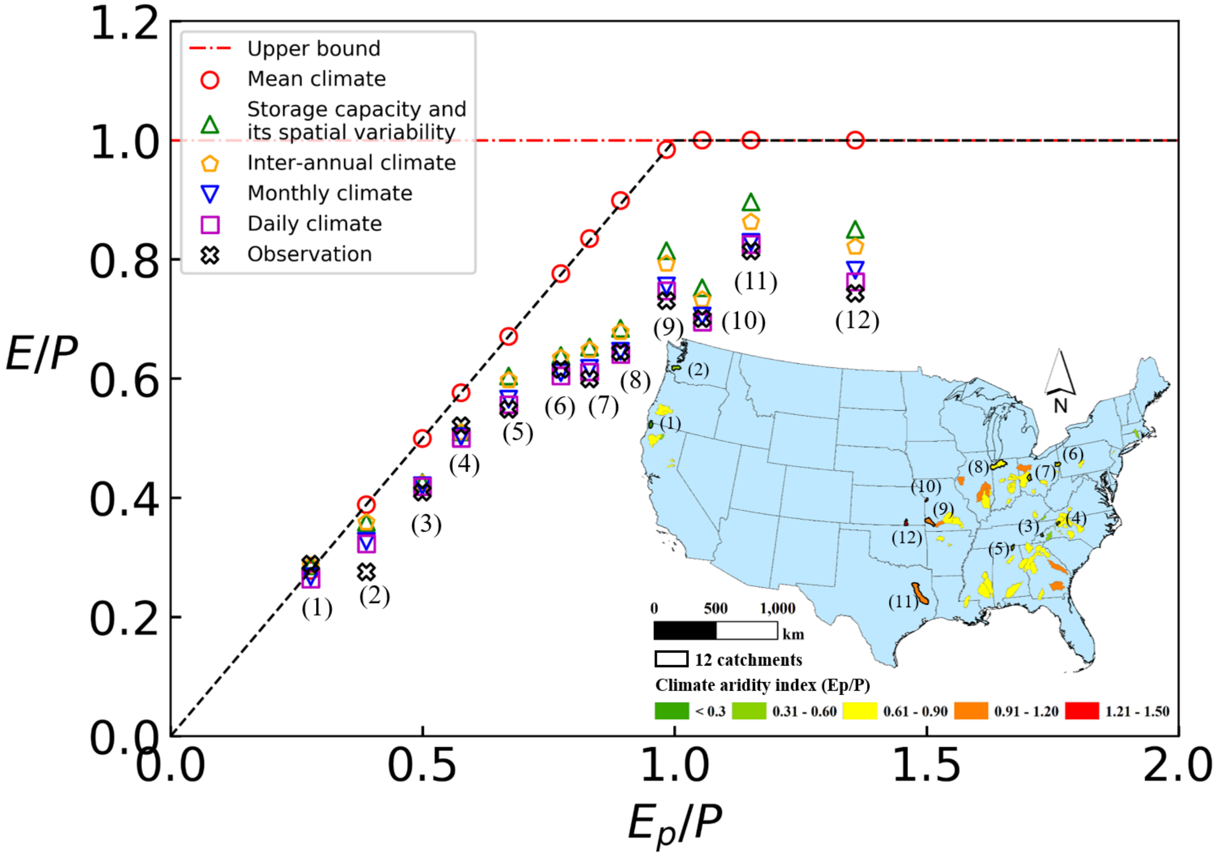

Upper bound
Mean climate
Storage capacity and its spatial variability
Inter-annual climate
Monthly climate
Daily climate
Observation
E/P
Ep/P
0.0
0.2
0.4
0.6
0.8
1.0
1.2
0.0
0.5
1.0
1.5
2.0
(1)
(2)
(3)
(4)
(5)
(6)
(7)
(8)
(9)
(10)
(11)
(12)
N
0 500 1,000
km
12 catchments
Climate aridity index (Ep/P)
< 0.3
0.31 - 0.60
0.61 - 0.90
0.91 - 1.20
1.21 - 1.50

Figure 11.

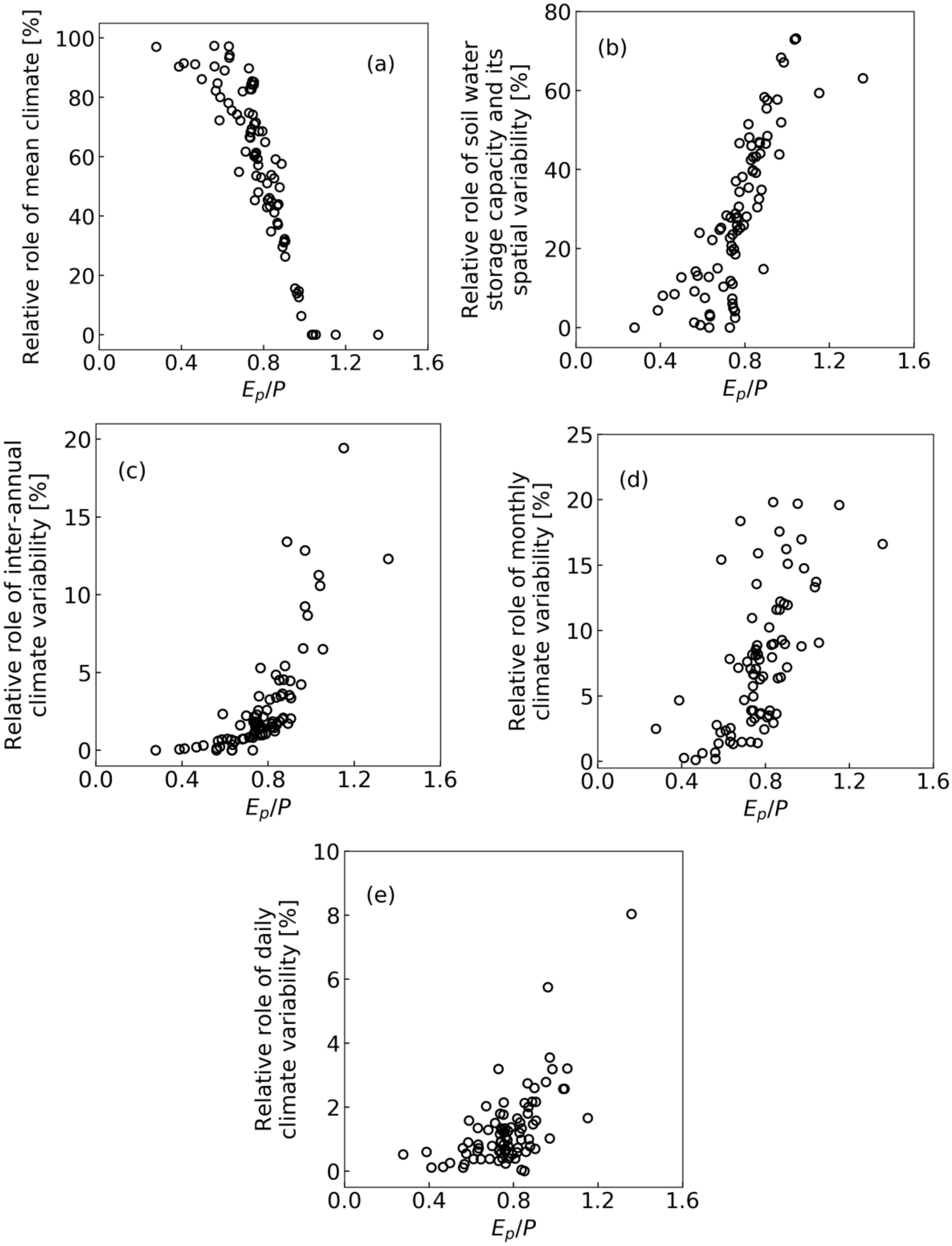
(a)
Relative role of mean climate [%]
E_p/P
(b)
Relative role of soil water storage capacity and its spatial variability [%]
E_p/P
(c)
Relative role of inter-annual climate variability [%]
E_p/P
(d)
Relative role of monthly climate variability [%]
E_p/P
(e)
Relative role of daily climate variability [%]
E_p/P

Figure 12.

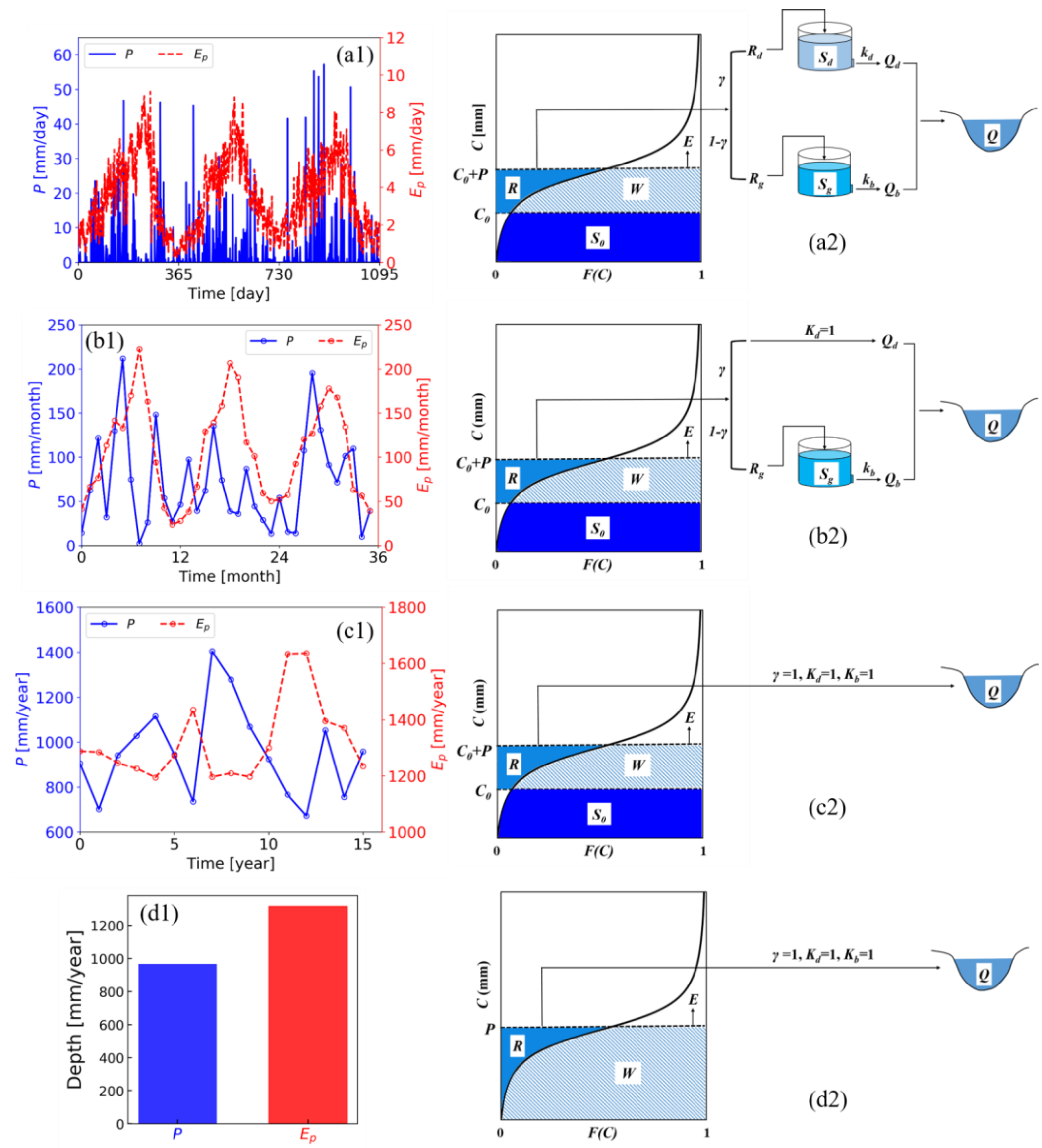

(a1)
P [mm/day]
Ep [mm/day]
Time [day]
(a2)
C [mm]
F(C)
C0+P
C0
R
W
S0
E
γ
1-γ
Rd
Rg
Sd
Sg
kd
kb
Qd
Qb
Q
(b1)
P [mm/month]
Ep [mm/month]
Time [month]
(b2)
C (mm)
Kd=1
(c1)
P [mm/year]
Ep [mm/year]
Time [year]
(c2)
γ =1, Kd=1, Kb=1
(d1)
Depth [mm/year]
P
Ep
(d2)

Index	USGS gage number	Parameter and range				
		S_b [mm]	a [-]	γ [-]	k_b [day^{-1}]	k_d [day^{-1}]
		[50-1500]	(0-2)	[0-1]	[0-0.14)	[0.14-1]
(1)	11532500	1366.7	1.9979	0.8689	0.0002	0.2509
(2)	12027500	775.2	1.9841	0.9989	0.1388	0.1741
(3)	03512000	581.3	1.9396	0.6140	0.0306	0.2703
(4)	03161000	531.5	1.9726	0.5727	0.0069	0.2788
(5)	03574500	370.7	1.9866	0.9990	0.1324	0.2540
(6)	03109500	410.3	1.9631	0.9990	0.1133	0.2042
(7)	03269500	335.9	1.9464	0.5782	0.0052	0.2554
(8)	05520500	295.1	1.9439	0.3364	0.0122	0.1402
(9)	07186000	441.0	1.9858	0.9988	0.1376	0.2928
(10)	06894000	293.9	1.9403	0.9999	0.0829	0.3735
(11)	08033500	878.7	1.9888	0.0014	0.0810	0.1628
(12)	07172000	235.6	1.9419	0.9989	0.1345	0.3622